

The virtual element method for the coupled system of magneto-hydrodynamics

S. Naranjo Alvarez ^a V. Bokil ^b V. Gyrya ^c and G. Manzini ^d

^a *Department of Mathematics, Oregon State University, Corvallis, OR 97331 USA, e-mail: naranjos@math.oregonstate.edu*

^b *Department of Mathematics, Oregon State University, Corvallis, OR 97331 USA, e-mail: bokilv@math.oregonstate.edu*

^c *Group T-5, Theoretical Division, Los Alamos National Laboratory, Los Alamos, 87545 NM, USA;*

e-mail: vitaliy.gyrya@lanl.gov

^d *Group T-5, Theoretical Division, Los Alamos National Laboratory, Los Alamos, 87545 NM, USA;*

e-mail: gmanzini@lanl.gov

Abstract

In this work, we review the framework of the Virtual Element Method (VEM) for a model in magneto-hydrodynamics (MHD), that incorporates a coupling between electromagnetics and fluid flow, and allows us to construct novel discretizations for simulating realistic phenomenon in MHD. First, we study two chains of spaces approximating the electromagnetic and fluid flow components of the model. Then, we show that this VEM approximation will yield divergence free discrete magnetic fields, an important property in any simulation in MHD. We present a linearization strategy to solve the VEM approximation which respects the divergence free condition on the magnetic field. This linearization will require that, at each non-linear iteration, a linear system be solved. We study these linear systems and show that they represent well-posed saddle point problems. We conclude by presenting numerical experiments exploring the performance of the VEM applied to the subsystem describing the electromagnetics. The first set of experiments provide evidence regarding the speed of convergence of the method as well as the divergence-free condition on the magnetic field. In the second set we present a model for magnetic reconnection in a mesh that includes a series of hanging nodes, which we use to calibrate the resolution of the method. The magnetic reconnection phenomenon happens near the center of the domain where the mesh resolution is finer and high resolution is achieved.

1. Introduction

The number of applications involving electrically charged and magnetized fluids, for example plasmas, has “skyrocketed” in the last decades and great efforts have been devoted to the development of predictive mathematical models. One approach that has withstood the test of time and has become “standard” in the area of plasma physics is the area called Magneto-HydroDynamics (MHD), which studies the behavior and the magnetic properties of electrically conducting fluids. The system of equations that describe MHD are a coupling between an electromagnetic submodel and a fluid flow submodel. The electromagnetic submodel in MHD is normally based on Maxwell’s equations while the fluid flow submodel relies on conservation principles such as mass and momentum conservation. These two submodels are nonlinearly coupled. Indeed, mass density and momentum distribution in a plasma are determined by the Lorentz force, which, in turn, is generated by the same plasma particles moving in the self-consistent electromagnetic field. The details of the MHD model, its derivation and properties are nowadays well-understood and explained in many textbooks and review papers, e.g., [38, 60].

The topic of this chapter is the review of a novel discretization method for an MHD model, in the framework of the Virtual Element Method (VEM), that has been recently proposed [62]. In the development of this method we will fix the approximation degree.

VEM was originally proposed as a variational reformulation of the *nodal* mimetic finite difference (MFD) method [27, 12] for solving diffusion problems on unstructured polygonal meshes in a finite element setting. A survey of the MFD method can be found in the review paper [51] and the research monograph [13].

Solving partial differential equations (PDEs) on polygonal and polyhedral meshes has become a central and important issue in the last decades. In fact, the generality of the admissible meshes makes the VEM highly versatile and very useful when the mesh must be adapted to the characteristics of the problem. For example, we can mention problems where the domain boundary deforms in time, or there are oddly shaped material interfaces to which the mesh must be conformal, or the mesh needs to be locally refined in those parts of the domain requiring greater accuracy as in adaptive mesh refinement strategies. In all such situations, the mesh refinement process may result in highly skewed meshes or meshes with highly irregular structures and a numerical method must be capable of handling these traits in order to be robust and provide an accurate approximation to the solution of a partial differential equation.

The VEM inherits the great mesh flexibility of the MFD in a setting similar to the finite element method (FEM), so that results and techniques from FEM can be imported over to VEM. Moreover, VEM makes possible to formulate numerical approximations of arbitrary order and arbitrary regularity to PDEs in two and three dimensions on meshes that other methods often consider as pathological. Because of its origins, VEM is intimately connected with other finite element approaches and the fact that VEM is a FEM implies some important advantages over other discretization methods such as the finite volume methods and the finite difference methods. The connection between VEM and finite elements on polygonal/polyhedral meshes was thoroughly investigated in [56, 30, 40], between VEM and discontinuous skeletal gradient discretizations in [40], and between VEM and BEM-based FEM method in [29].

The main difference between VEM and FEM is that VEM does not require an explicit knowledge of basis functions that generates the finite element approximation space. The formulation of the method and its practical implementations are based on suitable polynomial projections that are always computable from a careful choice of the degrees of freedom. VEM was first proposed for the Poisson equation [4] and, then, extended to convection-reaction-diffusion problems with variable coefficients in [10]. The effectiveness of the virtual element approach is reflected in the many significant applications that have been developed in less than a decade see, for example, [17, 20, 59, 64, 2, 11, 10, 28, 65, 69, 55, 32, 37, 19, 3, 31]. Numerical dispersion can also be greatly reduced on carefully selected polygonal meshes, see [47, 41]. In these works, the Finite Difference Time Domain (FDTD) method is applied to a grid of hexagonal prisms and yields much less numerical dispersion and anisotropy than on using regular hexahedral grids where such method is normally considered.

Finally, the divergence of the magnetic field is zero in the Maxwell equations thus reflecting the absence of magnetic monopoles. Classical numerical discretizations fail to capture this property when the discrete versions of the divergence and rotational operators do not annihilate each other at the level of the zero machine precision, thus leaving a remainder that can significantly be compounded during a simulation. The consequence of the violation of this divergence-free constraint has thoroughly been investigated in the literature and it was seen that the numerical simulations are prone to significant errors [23, 22, 36, 67], as fictitious forces and an unphysical behavior may appear [36]. Efforts have been devoted to the development of *divergence-free* techniques. For example, in [39] the divergence equation $\nabla \cdot \mathbf{B} = 0$ is taken into account through a Lagrange multiplier that is additionally introduced in the set of the unknowns; in [50], the divergence-free condition relies on special flux limiters; in [46] a special energy functional is minimized by a least squares finite element method. Instead, the VEM considered in this chapter provides a numerical approximation of the magnetic field that is intrinsically divergence free as a consequence of a de Rham inequality chain. The VEM described in the papers of References [5, 6, 18] are also pertinent to this issue.

This chapter is structured as follows. In Section 2, we present the system of equations of the continuous MHD model and introduce its discrete virtual element approximation. In Section 3, we review the formal definition and properties of the finite dimensional functional spaces of the formulation of VEM. Here, we also discuss the computability of the orthogonal projection operators and the possibility of using oblique projection operators, which are orthogonal with respect to a different inner product. In Section 4, we present a number of energy estimates that provide evidence of the stability of the method. In Section 4, we review a possible linearization strategy for solving the nonlinear system that results from virtual element approximation of the MHD model and prove that the approximate magnetic field is divergence free. In Section 5, we discuss the well-posedness of the linear solver in the setting of saddle-point

problems. In Section 6, we assess the convergence behavior of the method and show an application of the VEM to the numerical modeling of a magnetic reconnection phenomenon. Finally, in Section 7, we give the full picture about the proposed method we outline.

2. Mathematical Formulation

Let the computational domain \mathcal{D} be an open, bounded, polygonal subset of \mathbb{R}^3 . Further assume that there is a magnetized fluid contained in this domain. We denote by \vec{u} , \vec{B} , \vec{E} and p the velocity, magnetic and electric fields and the pressure of such a fluid. The evolution of these quantities is governed by the following system of differential equations:

$$\text{Incompressibility of the fluid : } \nabla \cdot \vec{u} = 0, \quad (1a)$$

$$\text{Conservation of momentum : } \frac{\partial}{\partial t} \vec{u} - R_e^{-1} \Delta \vec{u} - \vec{J} \times \vec{B} + \nabla p = \vec{f}, \quad (1b)$$

$$\text{Faraday's Law : } \frac{\partial}{\partial t} \vec{B} + \nabla \times \vec{E} = \vec{0}, \quad (1c)$$

$$\text{Ohm's Law : } \vec{J} = \vec{E} + \vec{u} \times \vec{B}, \quad (1d)$$

$$\text{Ampère's Law : } \vec{J} - R_m^{-1} \nabla \times \vec{B} = \vec{0}, \quad (1e)$$

We denote the two dimensional vector whose components are the x, y components of a three dimensional vector using bold. Thus we denote

$$\vec{B} = \begin{pmatrix} \mathbf{B} \\ B_z \end{pmatrix}, \quad \vec{E} = \begin{pmatrix} \mathbf{E} \\ E_z \end{pmatrix}, \quad \vec{u} = \begin{pmatrix} \mathbf{u} \\ u_z \end{pmatrix}, \quad \vec{J} = \begin{pmatrix} \mathbf{J} \\ J_z \end{pmatrix}, \quad \vec{f} = \begin{pmatrix} \mathbf{f} \\ f_z \end{pmatrix}.$$

In this chapter we will consider that the z -component of the magnetic field is exactly zero. Moreover, we will also consider that the x and y components of the magnetic and electric fields and the z -component of the velocity field do not vary in the z -direction. In summary, we are assuming that

$$B_z = \frac{\partial}{\partial z} \mathbf{B} = \frac{\partial}{\partial z} \mathbf{E} = \frac{\partial}{\partial z} u_z = 0.$$

The consequence is that the dynamics only occurs in two dimensions effectively reducing the dimensionality of the problem. Our goal will be to attain approximations to the x and y components of the electric and magnetic fields.

Consider an arbitrary, non-empty, cross-section parallel to the x, y -plane of \mathcal{D} denoted by Ω . The domain Ω is embedded in \mathbb{R}^2 so each point $p \in \Omega$ has a fixed z -value. Applying the aforementioned set of assumptions allows us to predict the dynamics in Ω as being ruled by:

$$\text{Incompressibility of the fluid : } \operatorname{div} \mathbf{u} = 0, \quad (2a)$$

$$\text{Conservation of momentum : } \frac{\partial}{\partial t} \mathbf{u} - R_e^{-1} \Delta \mathbf{u} - \mathbf{J} \times \mathbf{B} + \nabla p = \mathbf{f}, \quad (2b)$$

$$\text{Faraday's Law : } \frac{\partial}{\partial t} \mathbf{B} + \operatorname{rot} \mathbf{E} = \mathbf{0}, \quad (2c)$$

$$\text{Ohm's Law : } \mathbf{J} = \mathbf{E} + \mathbf{u} \times \mathbf{B}, \quad (2d)$$

$$\text{Ampère's Law : } \mathbf{J} - R_m^{-1} \operatorname{rot} \mathbf{B} = \mathbf{0}, \quad (2e)$$

Consider a scalar function $f : \Omega \rightarrow \mathbb{R}$ and vector functions

$$\mathbf{g}, \mathbf{f} : \Omega \rightarrow \mathbb{R}^2, \quad \text{where } \mathbf{f} = \begin{pmatrix} f_x \\ f_y \end{pmatrix}, \quad \mathbf{g} = \begin{pmatrix} g_x \\ g_y \end{pmatrix},$$

with the sub-indices denoting components of the vector values functions \mathbf{f} and \mathbf{g} , rather than differentiation. We define two versions of a cross product:

$$\mathbf{f} \times \mathbf{g} = \begin{pmatrix} -f_y g_x \\ f_x g_y \end{pmatrix}, \quad \mathbf{f} \times \mathbf{g} = f_x g_y - f_y g_x. \quad (3)$$

The two dimensional curl and divergence operators are defined as:

$$\mathbf{rot} E = \begin{pmatrix} \frac{\partial}{\partial y} E \\ -\frac{\partial}{\partial x} E \end{pmatrix}, \quad \mathbf{rot} \mathbf{B} = \frac{\partial}{\partial x} B_y - \frac{\partial}{\partial y} B_x \quad \text{and} \quad \mathbf{div} \mathbf{u} = \frac{\partial}{\partial x} u_x + \frac{\partial}{\partial y} u_y.$$

The initial conditions we prescribe onto the system are:

$$\mathbf{u}(0) = \mathbf{u}_0 \quad \text{and} \quad \mathbf{B}(0) = \mathbf{B}_0. \quad (4)$$

The initial field \mathbf{B}_0 must be divergence free, as Gauss's Law for the magnetic field requires that \mathbf{B} remain divergence free throughout its evolution. Gauss's law, i.e., the divergence free nature of \mathbf{B} , is not explicitly stated in the system of MHD equations. This is due to the fact that, under the assumption that \mathbf{B}_0 is divergence free, $\mathbf{div} \mathbf{B} = 0$ is a consequence of Faraday's Law, implying that \mathbf{B} is solenoidal for all time. We have

$$\frac{\partial}{\partial t} (\mathbf{div} \mathbf{B}) = \mathbf{div} \left(\frac{\partial}{\partial t} \mathbf{B} \right) = \mathbf{div} (-\mathbf{rot} E) = 0. \quad (5)$$

Hence,

$$\mathbf{div} \mathbf{B} = \mathbf{div} \mathbf{B}_0 = 0. \quad (6)$$

Such condition is a further evidence of the fact that the magnetic field is divergence free and the violation of this condition will lead to a nonphysical description of a MHD phenomenon.. We close the MHD system by adding the boundary conditions

$$\mathbf{u} = \mathbf{u}_b \quad \text{and} \quad E = E_b \quad \text{on } \partial\Omega. \quad (7)$$

On using the divergence theorem and the incompressibility condition, we find that

$$\int_{\partial\Omega} \mathbf{u} \cdot \mathbf{n} \, d\ell = \int_{\Omega} \mathbf{div} \mathbf{u} \, dA = 0, \quad (8)$$

which implies the consistency condition

$$\int_{\partial\Omega} \mathbf{u}_b \cdot \mathbf{n} \, d\ell = 0 \quad (9)$$

on the boundary velocity field \mathbf{u}_b .

2.1. Weak formulation

In this section, we present a weak formulation of problem (2). Such a formulation requires the definition of the following inner products and norms.

We use standard notation that, for the sake of completeness, we will describe in what follows. For a pair of sufficiently regular real-valued functions $f, g : \Omega \rightarrow \mathbb{R}$ or vector valued-functions $\mathbf{f}, \mathbf{g} : \Omega \rightarrow \mathbb{R}^2$ we define

$$(f, g) = \int_{\Omega} f g \, dx, \quad (\mathbf{f}, \mathbf{g}) = \int_{\Omega} \mathbf{f} \cdot \mathbf{g} \, dx. \quad (10)$$

We will denote the L^2 -norms by

$$\|f\|_{0,\Omega} := \left(\int_{\Omega} |f|^2 \, dx \right)^{1/2}, \quad (11a)$$

$$\|\mathbf{f}\|_{0,\Omega} := \left(\int_{\Omega} |\mathbf{f}|^2 \, dx \right)^{1/2}. \quad (11b)$$

The spaces $L^2(\Omega)$ and $[L^2(\Omega)]^2$ will consist of all those scalar and vector functions, respectively, that have finite L^2 -norms. Likewise, the H^1 -norm and the corresponding spaces $H^1(\Omega)$ and $[H^1(\Omega)]^2$ are defined below. We have

$$\|f\|_{1,\Omega} := (\|f\|_{0,\Omega}^2 + \|\nabla f\|_{0,\Omega}^2)^{1/2}, \quad (12a)$$

$$\|\mathbf{f}\|_{1,\Omega} := (\|\mathbf{f}\|_{0,\Omega}^2 + \|\nabla \mathbf{f}\|_{0,\Omega}^2)^{1/2}. \quad (12b)$$

The setting, in space, will require the following functional spaces:

$$H^1(\Omega) = \{v \in L^2(\Omega) : \nabla v \in [L^2(\Omega)]^2\}, \quad (13a)$$

$$H(\mathbf{rot}; \Omega) = \{D \in L^2(\Omega) : \mathbf{rot} D \in [L^2(\Omega)]^2\}, \quad (13b)$$

$$H(\text{div}; \Omega) = \{\mathbf{C} \in [L^2(\Omega)]^2 : \text{div} \mathbf{C} \in L^2(\Omega)\}, \quad (13c)$$

$$L_0^2(\Omega) = \left\{q \in L^2(\Omega) : \int_{\Omega} q \, dA = 0\right\}, \quad (13d)$$

$$H_0^1(\Omega) = \{v \in H^1 : v|_{\partial\Omega} = 0\}, \quad (13e)$$

$$H_0(\mathbf{rot}; \Omega) = \{D \in H(\mathbf{rot}; \Omega) : D|_{\partial\Omega} = 0\}, \quad (13f)$$

Each of the function spaces in (13) are endowed with its natural norm. Let us refer to a generic version of the space from (13) as $S(\Omega)$ and to its natural norm as $\|\cdot\|_S$. We say that a function $f : [0, T] \rightarrow S(\Omega)$ is continuous in time if it is continuous with respect to the natural norm $\|\cdot\|_S$. The space of all time continuous functions $f : [0, T] \rightarrow S(\Omega)$ is denoted as $C(0, T; S(\Omega))$. Thus,

$$C^1(0, T; [H^1(\Omega)]^2) = \left\{\mathbf{v} : [0, T] \rightarrow [H^1(\Omega)]^2 : \mathbf{v} \text{ and } \frac{\partial \mathbf{v}}{\partial t} \text{ are continuous}\right\}, \quad (14a)$$

$$C(0, T; L_0^2(\Omega)) = \{q : [0, T] \rightarrow L_0^2(\Omega) : q \text{ is continuous}\}, \quad (14b)$$

$$C(0, T; H(\mathbf{rot}; \Omega)) := \{E : [0, T] \rightarrow H(\mathbf{rot}; \Omega) : E \text{ is continuous}\}, \quad (14c)$$

$$C^1(0, T; H(\text{div}; \Omega)) = \left\{\mathbf{B} : [0, T] \rightarrow H(\text{div}; \Omega) : \right. \\ \left. \mathbf{B} \text{ and } \frac{\partial}{\partial t} \mathbf{B} \text{ are continuous}\right\}. \quad (14d)$$

The weak form of problem (2a)-(2e) reads as:

Find

$$\mathbf{u} \in C^1(0, T; [H^1(\Omega)]^2), \quad \mathbf{B} \in C^1(0, T; H(\text{div}; \Omega)),$$

$$E \in C(0, T; H_0(\mathbf{rot}; \Omega)), \quad p \in C(0, T; L_0^2(\Omega)),$$

such that

$$\left(\frac{\partial}{\partial t} \mathbf{u}, \mathbf{v}\right) + R_e^{-1}(\nabla \mathbf{u}, \nabla \mathbf{v}) - (J \times \mathbf{B}, \mathbf{v}) - (p, \text{div} \mathbf{v}) = (\mathbf{f}, \mathbf{v}), \quad (15a)$$

$$(\text{div} \mathbf{u}, q) = 0, \quad (15b)$$

$$\left(\frac{\partial}{\partial t} \mathbf{B}, \mathbf{C}\right) + (\mathbf{rot} E, \mathbf{C}) = 0, \quad (15c)$$

$$(J, D) - R_m^{-1}(\mathbf{B}, \mathbf{rot} D) = 0, \quad (15d)$$

$$J = E + \mathbf{u} \times \mathbf{B}, \quad \mathbf{u}(\cdot, 0) = \mathbf{u}_0, \quad \mathbf{B}(\cdot, 0) = \mathbf{B}_0 \text{ with } \text{div} \mathbf{B}_0 = 0, \quad (15e)$$

for any $\mathbf{v} \in [H_0^1(\Omega)]^2$, $\mathbf{C} \in H(\text{div}; \Omega)$, $D \in H_0(\mathbf{rot}; \Omega)$, and $q \in L_0^2(\Omega)$. In this formulation we are making implicit that

$$\mathbf{u} = \mathbf{u}_b \quad \text{and} \quad E = E_b \quad \text{along} \quad \partial\Omega. \quad (16)$$

3. The Virtual Element Method

In the VEM formulation, that will be presented, we will define conforming finite-dimensional subspaces of the spaces in (13). To do this we introduce a mesh of the domain Ω with size $h > 0$. Then, we define mesh-dependent finite dimensional virtual element spaces:

$$\mathcal{P}_h \subset L^2(\Omega), \quad \mathcal{V}_h \subset H(\mathbf{rot}; \Omega), \quad \mathcal{E}_h \subset H(\text{div}; \Omega) \quad \mathcal{TV}_h \subset [H^1(\Omega)]^2. \quad (17a)$$

$$\mathcal{P}_{h,0} \subset L_0^2(\Omega), \quad \mathcal{V}_{h,0} \subset H_0(\mathbf{rot}; \Omega), \quad \mathcal{TV}_{h,0} \subset [H_0^1(\Omega)]^2, \quad (17b)$$

with the obvious inclusions

$$\mathcal{TV}_{h,0} \subset \mathcal{TV}_h, \quad \mathcal{V}_{h,0} \subset \mathcal{V}_h, \quad \mathcal{P}_{h,0} \subset \mathcal{P}_h. \quad (18)$$

These spaces will be formally defined in Subsections 3.2, 3.3, 3.4 and 3.6, respectively. We endow these finite dimensional spaces with the inner products

$$(\mathbf{u}_h, \mathbf{v}_h)_{\mathcal{TV}_h} \approx (\mathbf{u}_h, \mathbf{v}_h), \quad [\mathbf{u}_h, \mathbf{v}_h]_{\mathcal{TV}_h} \approx (\nabla \mathbf{u}_h, \nabla \mathbf{v}_h), \quad (19a)$$

$$(\mathbf{B}_h, \mathbf{C}_h)_{\mathcal{E}_h} \approx (\mathbf{B}_h, \mathbf{C}_h), \quad (E_h, D_h)_{\mathcal{V}_h} \approx (E_h, D_h), \quad (19b)$$

$$(p_h, q_h)_{\mathcal{P}_h} \approx (p_h, q_h), \quad (19c)$$

which approximate the corresponding inner products in $L^2(\Omega)$ and $H^1(\Omega)$ and their vector variants. In the formulation of the method, we will find it convenient to use a set of local and global interpolation operators embedding the continuous spaces into their discrete versions. We denoted the local operators referring to a specific mesh element P as $\mathcal{I}_P^{\mathcal{TV}_h}$, $\mathcal{I}_P^{\mathcal{E}_h}$, $\mathcal{I}_P^{\mathcal{V}_h}$ and $\mathcal{I}^{\mathcal{P}_h}$ and the corresponding global ones $\mathcal{I}^{\mathcal{TV}_h}$, $\mathcal{I}^{\mathcal{E}_h}$, $\mathcal{I}^{\mathcal{V}_h}$ and $\mathcal{I}^{\mathcal{P}_h}$.

Having defined the functional spaces, we now turn our attention to the time variable. To begin we introduce a time-step $\Delta t > 0$ and the time staggering parameter $0 \leq \theta \leq 1$. The approximate solutions will be considered at time steps given by

$$t^n = n\Delta t, \quad t^{n+\theta} = (n + \theta)\Delta t.$$

These approximations are abbreviated by $\mathbf{u}_h^n = \mathbf{u}_h(\cdot, t^n)$, $p_h^{n+\theta} = p_h(\cdot, t^{n+\theta})$, $\mathbf{B}_h^n = \mathbf{B}_h(\cdot, t^n)$, and $E_h^{n+\theta} = E_h(\cdot, t^{n+\theta})$ for the time-dependent vector fields \mathbf{u}_h and \mathbf{B}_h and the scalar fields E_h and p_h , respectively, approximating \mathbf{u} , \mathbf{B} , E and p . These vector fields are the solution of the virtual element method, which reads as:

Find $\{(\mathbf{u}_h^n, \mathbf{B}_h^n)\}_{n=0}^N \subset \mathcal{TV}_h \times \mathcal{E}_h$ and $\{(E_h^{n+\theta}, p_h^{n+\theta})\}_{n=0}^{N-1} \subset \mathcal{V}_h \times \mathcal{P}_{h,0}$, such that

$$\begin{aligned} \left(\frac{\mathbf{u}_h^{n+1} - \mathbf{u}_h^n}{\Delta t}, \mathbf{v}_h \right)_{\mathcal{TV}_h} + R_e^{-1} [\mathbf{u}_h^{n+\theta}, \mathbf{v}_h]_{\mathcal{TV}_h} + \underbrace{\left(J_h^{n+\theta}, \mathcal{I}^{\mathcal{V}_h}(\mathbf{v}_h \times \Pi^{RT} \mathbf{B}_h^{n+\theta}) \right)_{\mathcal{V}_h}}_{(*)} \\ - \left(p_h^{n+\theta}, \text{div} \mathbf{v}_h \right)_{\mathcal{P}_h} = \left(\mathbf{f}_h, \mathbf{v}_h \right)_{\mathcal{TV}_h}, \end{aligned} \quad (20a)$$

$$\left(\text{div} \mathbf{u}_h^{n+\theta}, q_h \right)_{\mathcal{P}_h} = 0, \quad (20b)$$

$$\left(\frac{\mathbf{B}_h^{n+1} - \mathbf{B}_h^n}{\Delta t}, \mathbf{C}_h \right)_{\mathcal{E}_h} + \left(\mathbf{rot} E_h^{n+\theta}, \mathbf{C}_h \right)_{\mathcal{E}_h} = 0, \quad (20c)$$

$$\left(J_h^{n+\theta}, D_h \right)_{\mathcal{V}_h} - R_m^{-1} (\mathbf{B}_h^{n+\theta}, \mathbf{rot} D_h)_{\mathcal{E}_h} = 0, \quad (20d)$$

for all $\mathbf{v}_h \in \mathcal{TV}_{h,0}$, $\mathbf{C}_h \in \mathcal{E}_h$, $D_h \in \mathcal{V}_{h,0}$ and $q_h \in \mathcal{P}_{h,0}$. We define

$$J_h^{n+\theta} := E_h^{n+\theta} + \mathcal{I}^{\mathcal{V}_h}(\mathbf{u}_h^{n+\theta} \times \Pi^{RT} \mathbf{B}_h^{n+\theta}), \quad (21)$$

and the fractional step quantities $\mathbf{u}_h^{n+\theta}$, $\mathbf{B}_h^{n+\theta}$ through linear (in time) interpolations

$$\mathbf{u}_h^{n+\theta} := (1 - \theta)\mathbf{u}_h^n + \theta\mathbf{u}_h^{n+1}, \quad (22a)$$

$$\mathbf{B}_h^{n+\theta} := (1 - \theta)\mathbf{B}_h^n + \theta\mathbf{B}_h^{n+1}. \quad (22b)$$

The initial conditions are given as

$$\mathbf{u}_h^0 = \mathcal{I}^{\mathcal{V}_h}(\mathbf{u}_0), \quad \mathbf{B}_h^0 = \mathcal{I}^{\mathcal{E}_h}(\mathbf{B}_0) \quad \text{with} \quad \operatorname{div} \mathbf{B}_0 = 0. \quad (23)$$

Here, we implicitly assume that for all $t \in [0, T]$:

$$E_h(t) = \mathcal{I}^{\mathcal{V}_h}(E_b(t)) \quad \text{and} \quad \mathbf{u}_h(t) = \mathcal{I}^{\mathcal{V}_h}(\mathbf{u}_b(t)) \quad \text{along} \quad \partial\Omega.$$

Here we use E_b and \mathbf{u}_b as the extensions to the continuous boundary conditions to the interior of Ω .

The term labeled as (*) in (20a) is produced by the approximation

$$-(J \times \mathbf{B}, \mathbf{v}) = (J, \mathbf{v} \times \mathbf{B}) \approx (J_h, \mathcal{I}^{\mathcal{V}_h}(\mathbf{v}_h \times \mathbf{B}_h))_{\mathcal{V}_h}.$$

The reason why we use this discretization will be made clear in Section 4, where we present the stability estimates in the $L^2(\Omega)$ norm. It is important to note that when $\theta = 0$ the scheme, in time, is a forward Euler step. Whereas if $\theta = 1$ the scheme is a Backward Euler step.

3.1. Mesh notation and regularity assumptions

In this subsection, we present the main notation and the regularity assumptions that we will make on the mesh.

For ease of exposition, we assume that the computational domain Ω be an open, bounded, connected subset of \mathbb{R}^2 with polygonal boundary Γ . We consider the family of domain partitionings $\mathcal{T} = \{\Omega_h\}_{h \in \mathcal{H}}$. Every partition Ω_h , the *mesh*, is a finite collection of polygonal elements \mathbf{P} , which are such that $\bar{\Omega} = \cup_{\mathbf{P} \in \Omega_h} \bar{\mathbf{P}}$.

For a polygonal element $\mathbf{P} \in \Omega_h$, we denote the boundary of \mathbf{P} by $\partial\mathbf{P}$, the outward unit normal to the boundary by $\mathbf{n}_{\mathbf{P}}$, its diameter by $h_{\mathbf{P}} = \max_{\mathbf{x}, \mathbf{y} \in \mathbf{P}} |\mathbf{x} - \mathbf{y}|$, and its area by $|\mathbf{P}|$. Each elemental boundary $\partial\mathbf{P}$ is formed by a sequence of one-dimensional non-intersecting straight edges \mathbf{e} with length $h_{\mathbf{e}}$ and midpoint $\mathbf{x}_{\mathbf{e}} = (x_{\mathbf{e}}, y_{\mathbf{e}})^T$.

To enforce mesh regularity we require that there exists $\rho \geq 0$ independent of the mesh size $h > 0$, such that

(M1): every polygonal cell $\mathbf{P} \in \Omega_h$ is star-shaped with respect to every point of some disk of radius $\rho h_{\mathbf{P}}$;

(M2): every edge $\mathbf{e} \in \partial\mathbf{P}$ of cell $\mathbf{P} \in \Omega_h$ satisfies $h_{\mathbf{e}} \geq \rho h_{\mathbf{P}}$.

The regularity assumptions (M1)-(M2) allow us to use meshes with cells having quite general geometric shapes. For example, non-convex cells or cells with hanging nodes on their edges are admissible. Nonetheless, these assumptions have some important implications such as: (i) every polygonal element is *simply connected*; (ii) the number of edges of each polygonal cell in the mesh family $\{\Omega_h\}_h$ is uniformly bounded; (iii) a polygonal element cannot have *arbitrarily small* edges with respect to its diameter $h_{\mathbf{P}} \leq h$ for $h \rightarrow 0$ and inequality $h_{\mathbf{P}}^2 \leq C(\rho)|\mathbf{P}|h_{\mathbf{P}}^2$ holds, with the obvious dependence of constant $C(\rho)$ on the mesh regularity factor ρ .

Remark 3.1 *It is worth mentioning that virtual element methods on polygonal meshes possibly containing “small edges” have been considered in [25] for the numerical approximation of the Poisson problem. The work in [25] extends the results in [14] for the original two-dimensional virtual element method to the version of the virtual element method in [1] that can also be applied to problems in three dimensions, see [35]. Finally, we note that assumptions (M1)-(M2) above also imply that the classical polynomial approximation theory in Sobolev spaces holds [24]. While these assumptions are the minimal necessary to develop theoretical analysis, in practice they can be significantly weakened.*

3.2. The Nodal Space

Consider the cell \mathbf{P} of the polygonal mesh Ω_h . The formal definition of the nodal elemental space is

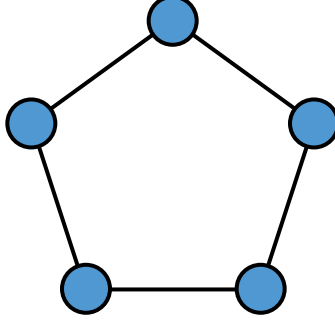


Fig. 1. Representation of the degrees of freedom of functions in $\mathcal{V}_h(\mathbf{P})$.

$$\mathcal{V}_h(\mathbf{P}) := \left\{ D_h \in H(\mathbf{rot}; \mathbf{P}) : D_h|_{\partial \mathbf{P}} \in C(\partial \mathbf{P}), D_h \in \mathbb{P}_1(\mathbf{e}) \ \forall \mathbf{e} \in \partial \mathbf{P}, \right. \quad (24)$$

$$\left. \text{rot rot } D_h = 0 \text{ in } \mathbf{P} \right\}. \quad (25)$$

Every function $D_h \in \mathcal{V}_h(\mathbf{P})$ is uniquely determined by the set of degrees of freedom:

(V) the vertex values $D_h(\mathbf{v})$ at the nodes \mathbf{v} of cell \mathbf{P} .

These are represented by blue disks centered at the nodes, see the sample picture in Figure 1.

As in the classic finite element method, this property is referred to as the *unisolvency* of the degrees of freedom (V), see [58]. Accordingly, every function in $\mathcal{V}_h(\mathbf{P})$ corresponds to one and only one set of degrees of freedom and, conversely, every set of degrees of freedom corresponds to one and only one function in $\mathcal{V}_h(\mathbf{P})$. To formally state this property we define the operators $\mathcal{R}_v : C^\infty(\Omega) \rightarrow \mathbb{R}^N$ such that for any $D \in C^\infty(\Omega)$ the image $\mathcal{R}_v(D)$ is the array of degrees of freedom of D . This function can be continuously extended to the full space $H(\mathbf{rot}; \mathbf{P})$. The next theorem states the unisolvency of the finite element previously described.

Theorem 3.2 Define $\mathcal{K}_v : \mathcal{V}_h(\mathbf{P}) \rightarrow \mathbb{R}^N$ as the restriction of \mathcal{R}_v to $\mathcal{V}_h(\mathbf{P})$. Then, \mathcal{K}_v is bijective.

Proof. Proof of the above theorem is provided in [9]. □

The result of Theorem 3.2 Allows us to define the mapping $\mathcal{I}_\mathbf{P}^{\mathcal{V}_h} : H(\mathbf{rot}; \mathbf{P}) \rightarrow \mathcal{V}_h(\mathbf{P})$ given by $\mathcal{I}_\mathbf{P}^{\mathcal{V}_h} = \mathcal{K}_v^{-1} \circ \mathcal{R}_v$.

We endow the space $\mathcal{V}_h(\mathbf{P})$ with an L^2 -like inner product. The usual strategy for the construction of an inner product in a finite dimensional space relies on the L^2 -orthogonal projection onto linear polynomials on \mathbf{P} , denoted by $\Pi_\mathbf{P}^0 : \mathcal{V}_h(\mathbf{P}) \rightarrow \mathbb{P}_1(\mathbf{P})$. Unfortunately, this projector is not computable in $\mathcal{V}_h(\mathbf{P})$. To have a computable orthogonal projection operator we could change the definition of the space as in the so called “enhancement approach” [8, 1, 9]. This strategy will, effectively, change the definition of the space $\mathcal{V}_h(\mathbf{P})$ calling into question whether or not an important De-Rham complex hold, see Subsection 3.5. The reality is that such a diagram holds even in the enhanced scenario, see [34]. However, we were not aware of this enhanced diagram, instead, we follow a different strategy through a special polynomial reconstruction operator $\Pi_\mathbf{P} : \mathcal{V}_h(\mathbf{P}) \rightarrow \mathbb{P}_1(\mathbf{P})$ satisfying the following three properties:

(P1) $\Pi_\mathbf{P} D_h$ is computable only from the degrees of freedom of $D_h \in \mathcal{V}_h(\mathbf{P})$;

(P2) $\Pi_\mathbf{P}$ preserves all linear polynomials, i.e., for any $D_h \in \mathbb{P}_1(\mathbf{P})$, $\Pi_\mathbf{P} D_h = D_h$;

(P3) $\Pi_\mathbf{P}$ is a bounded operator with respect to L^2 norm with the upper bound constant C_Π independent of the mesh resolution h , i.e., for any $D_h \in \mathcal{V}_h(\mathbf{P})$

$$\|\Pi_\mathbf{P} D_h\|_{0,\mathbf{P}} \leq C_\Pi \|D_h\|_{0,\mathbf{P}}. \quad (26)$$

We can use this projector to define an inner product in the space \mathcal{V}_h that will allow us to approximate L^2 -inner product as they appear in (20). In Subsection 3.2.1, we discuss three possible implementations of the polynomial reconstruction operator.

We define

$$(E_h, D_h)_{\mathcal{V}_h(\mathbf{P})} = (\Pi_\mathbf{P} E_h, \Pi_\mathbf{P} D_h) + \mathcal{S}^v((1 - \Pi_\mathbf{P}) E_h, (1 - \Pi_\mathbf{P}) D_h), \quad (27)$$

where \mathcal{S}^v is the stabilization bilinear form. According to the standard VEM construction, \mathcal{S}^v can be any bilinear form for which there exist two real constants s_* and s^* independent of h such that

$$s_* \|D_h\|_{0,\mathbf{P}}^2 \leq \mathcal{S}^\vee(D_h, D_h) \leq s^* \|D_h\|_{0,\mathbf{P}}^2 \quad \forall D_h \in \ker \Pi \cap \mathcal{V}_h(\mathbf{P}). \quad (28)$$

In practice, we can design the stabilization as in [57, 37]. This inner product defines the norm in $\mathcal{V}_h(\mathbf{P})$ given by $\|D_h\|_{\mathcal{V}_h(\mathbf{P})}^2 = (D_h, D_h)_{\mathcal{V}_h(\mathbf{P})}$. When the projection operator Π satisfies properties **(P1)**–**(P3)**, the inner product (27) satisfies two fundamental properties summarized in the following theorem.

Theorem 3.3 *The inner product $(\cdot, \cdot)_{\mathcal{V}_h(\mathbf{P})}$ defined in (27) satisfies*

– **Linear consistency**:

$$(p, q)_{\mathcal{V}_h(\mathbf{P})} = (p, q) \quad \forall p, q \in \mathbb{P}_1(\mathbf{P}) \subset \mathcal{V}_h(\mathbf{P}). \quad (29)$$

– **Stability**: *there exists two real constants α_* and $\alpha^* > 0$ independent of h and \mathbf{P} such that*

$$\alpha_* \|D_h\|_{0,\mathbf{P}}^2 \leq \|D_h\|_{\mathcal{V}_h(\mathbf{P})}^2 \leq \alpha^* \|D_h\|_{0,\mathbf{P}}^2 \quad \forall D_h \in \mathcal{V}_h(\mathbf{P})^2. \quad (30)$$

Proof. To prove the *linear consistency* (29), take two polynomial functions $p, q \in \mathbb{P}_1(\mathbf{P})$. Property **(P2)** implies that $\Pi p = p$ and $\Pi q = q$. So, the stabilization term in (27) is zero, and we find that

$$(p, q)_{\mathcal{V}_h(\mathbf{P})} = (\Pi p, \Pi q)_{\mathbf{P}} = (p, q)_{\mathbf{P}}.$$

To prove the lower bound of the *stability* condition (30), we add and subtract $\Pi_{\mathbf{P}} D_h$, apply the triangular inequality, the left-most inequality in (28) and note that

$$\begin{aligned} \|D_h\|_{0,\mathbf{P}}^2 &\leq (\|\Pi_{\mathbf{P}} D_h\|_{0,\mathbf{P}} + \|(1 - \Pi_{\mathbf{P}}) D_h\|_{0,\mathbf{P}})^2 \leq 2(\|\Pi_{\mathbf{P}} D_h\|_{0,\mathbf{P}}^2 + \|(1 - \Pi_{\mathbf{P}}) D_h\|_{0,\mathbf{P}}^2) \\ &\leq 2 \max(1, s^*) \left((\Pi_{\mathbf{P}} D_h, \Pi_{\mathbf{P}} D_h)_{\mathbf{P}} + \mathcal{S}^\vee((1 - \Pi_{\mathbf{P}}) D_h, (1 - \Pi_{\mathbf{P}}) D_h) \right) \\ &= (\alpha_*)^{-1} (D_h, D_h)_{\mathcal{V}_h(\mathbf{P})} = (\alpha_*)^{-1} \|D_h\|_{\mathcal{V}_h(\mathbf{P})}^2, \end{aligned}$$

where the lower bound α_* in (30) is given by $\alpha_*^{-1} = 2 \max(1, s^*)$.

To obtain the upper bound in (30), we first note that property **(P3)** implies that:

$$\begin{aligned} \mathcal{S}^\vee((1 - \Pi_{\mathbf{P}}) D_h, (1 - \Pi_{\mathbf{P}}) D_h) &\leq s^* \|(1 - \Pi_{\mathbf{P}}) D_h\|_{0,\mathbf{P}}^2 \leq s^* (\|D_h\|_{0,\mathbf{P}} + \|\Pi_{\mathbf{P}} D_h\|_{0,\mathbf{P}})^2 \\ &\leq s^* (\|D_h\|_{0,\mathbf{P}} + C_{\Pi} \|D_h\|_{0,\mathbf{P}})^2 \leq s^* (1 + C_{\Pi})^2 \|D_h\|_{0,\mathbf{P}}^2. \end{aligned}$$

To conclude this theorem we use

$$\begin{aligned} \|D_h\|_{\mathcal{V}_h(\mathbf{P})}^2 &= (\Pi_{\mathbf{P}} D_h, \Pi_{\mathbf{P}} D_h)_{\mathbf{P}} + \mathcal{S}^\vee((1 - \Pi_{\mathbf{P}}) D_h, (1 - \Pi_{\mathbf{P}}) D_h) \\ &\leq C_{\Pi}^2 \|D_h\|_{0,\mathbf{P}}^2 + s^* (1 + C_{\Pi})^2 \|D_h\|_{0,\mathbf{P}}^2 \leq \alpha^* \|D_h\|_{0,\mathbf{P}}^2, \end{aligned}$$

where the upper bound α^* in (30) is given by $\alpha^* = \max(C_{\Pi}^2, s^* (1 + C_{\Pi})^2)$.

Note that both lower and upper bounds α_* and α^* depend only on the upper bound C_{Π} of the projection operator Π and are independent of mesh resolution h . \square

The global space \mathcal{V}_h is the subset of functions in $H(\mathbf{rot}; \Omega)$ whose restriction to any element $\mathbf{P} \in \Omega_h$ belongs to $\mathcal{V}_h(\mathbf{P})$. Formally, we write that

$$\mathcal{V}_h = \{D_h \in H(\mathbf{rot}; \Omega) : \forall \mathbf{P} \in \Omega_h \quad D_h|_{\mathbf{P}} \in \mathcal{V}_h(\mathbf{P})\}. \quad (31)$$

We endow the global space \mathcal{V}_h with the global inner product

$$(E_h, D_h)_{\mathcal{V}_h} = \sum_{\mathbf{P} \in \Omega_h} (E_h|_{\mathbf{P}}, D_h|_{\mathbf{P}})_{\mathcal{V}_h(\mathbf{P})} \quad \forall E_h, D_h \in \mathcal{V}_h, \quad (32)$$

and the global norm $\|D_h\|_{\mathcal{V}_h}^2 = (D_h, D_h)_{\mathcal{V}_h}$. The global inner product inherits the properties of accuracy and stability from the elemental inner product that are stated in Theorem 3.3.

Corollary 3.4 *The inner product $(\cdot, \cdot)_{\mathcal{V}_h}$ defined in (32) has the two properties:*

– **Linear consistency**:

$$(p, q)_{\mathcal{V}_h} = (p, q) \quad \forall p, q \in \mathbb{P}_1(\Omega_h) \subset \mathcal{V}_h(\mathbf{P}). \quad (33)$$

– **Stability:** there exists two real constants α_* and $\alpha^* > 0$ independent of h and \mathbf{P} such that

$$\alpha_* \|D_h\|_0^2 \leq \|D_h\|_{\mathcal{V}_h(\mathbf{P})}^2 \leq \alpha^* \|D_h\|_0^2 \quad \forall D_h \in \mathcal{V}_h(\mathbf{P}), \quad (34)$$

where the lower and upper bound constants α_* and $\alpha^* > 0$ are the same constants introduced in Theorem 3.3 and $\mathbb{P}_1(\Omega_h)$ is the space of piecewise linear polynomials built on the mesh Ω_h .

Proof. Proof of this Corollary follows immediately from the results of Theorem [refThm:EquivalentInProdsVh\(P\)](#). \square

Finally, we introduce the *global interpolation operator* $\mathcal{I}^{\mathcal{V}_h} : H(\mathbf{rot}; \Omega) \rightarrow \mathcal{V}_h$, whose restriction to any cell coincides with the elemental interpolation operator:

$$\mathcal{I}^{\mathcal{V}_h}(D_h)|_{\mathbf{P}} = \mathcal{I}_{\mathbf{P}}^{\mathcal{V}_h}(D_h|_{\mathbf{P}}) \quad \forall D_h \in \mathcal{V}_h \quad \mathbf{P} \in \Omega_h. \quad (35)$$

3.2.1. The polynomial reconstruction operators

We discuss here three alternative choices for the oblique projections that can be used to approximate inner products in the space $\mathcal{V}_h(\mathbf{P})$.

(I) Elliptic Projection operator. We denote this projection operator as

$$\Pi_{\mathbf{P}}^{\mathbf{rot}} : \mathcal{V}_h(\mathbf{P}) \rightarrow \mathbb{P}_1(\Omega). \quad (36)$$

For $D_h \in \mathcal{V}_h(\mathbf{P})$ the elliptic projection operator is the solution to the variational problem

$$\int_{\mathbf{P}} \mathbf{rot} (D_h - \Pi_{\mathbf{P}}^{\mathbf{rot}} D_h) \cdot \mathbf{rot} q \, dA = 0 \quad \forall q \in \mathbb{P}_1(\mathbf{P}), \quad (37a)$$

$$P_0(D_h - \Pi_{\mathbf{P}}^{\mathbf{rot}} D_h) = 0, \quad (37b)$$

where we use the additional projector $P_0(D_h) = \sum_{\mathbf{v} \in \partial \mathbf{P}} D_h(\mathbf{v})$ on $\mathbb{P}_0(\mathbf{P})$ to remove the kernel of operator \mathbf{rot} . The linear polynomial $\Pi_{\mathbf{P}}^{\mathbf{rot}} D_h$ is computable because the integral quantities

$$\int_{\mathbf{P}} \mathbf{rot} D_h \cdot \mathbf{rot} q \, dA \quad \forall q \in \mathbb{P}_1(\mathbf{P}), \quad (38)$$

are computable from the degrees of freedom (\mathbf{V}) of D_h . To prove this statement we use the Green's theorem, note that $\mathbf{rot} \mathbf{rot} q = 0$, since $q \in \mathbb{P}_1(\mathbf{P})$, and split the integral on $\partial \mathbf{P}$ in the summation of edge integrals to obtain

$$\begin{aligned} \int_{\mathbf{P}} \mathbf{rot} D_h \cdot \mathbf{rot} q \, dA &= \int_{\mathbf{P}} D_h \mathbf{rot} \mathbf{rot} q \, dA + \int_{\partial \mathbf{P}} D_h \mathbf{t} \cdot \mathbf{rot} q \, d\ell \\ &= \sum_{\mathbf{e} \in \partial \mathbf{P}} \int_{\mathbf{e}} D_h \mathbf{t} \cdot \mathbf{rot} q \, d\ell, \end{aligned}$$

where \mathbf{t} is the unit tangent vector parallel to \mathbf{e} . The edge integrals are computable because $\mathbf{t} \cdot \mathbf{rot} q$ is a known function in $\mathbb{P}_0(\mathbf{e})$ and we can interpolate the trace $D_h|_{\mathbf{e}} \in \mathbb{P}_1(\mathbf{e})$ using the evaluation of D_h at the vertices of edge \mathbf{e} , which are known from the degrees of freedom (\mathbf{V}) .

(II) Least Squares polynomial reconstruction operator. The second reconstruction operator that we consider is denoted as

$$\Pi_{\mathbf{P}}^{LS} : \mathcal{V}_h(\mathbf{P}) \rightarrow \mathbb{P}_1(\Omega). \quad (39)$$

For a function $D_h \in \mathcal{V}_h(\mathbf{P})$, the linear polynomial $\Pi_{\mathbf{P}}^{LS} D_h$ is the solution of the Least Squares problem

$$\Pi_{\mathbf{P}}^{LS} D_h(\mathbf{x}) := \operatorname{argmin}_{q \in \mathbb{P}_1(\mathbf{P})} \sum_{\mathbf{v} \in \partial \mathbf{P}} |D_h(\mathbf{x}_{\mathbf{v}}) - q(\mathbf{x}_{\mathbf{v}})|^2.$$

The solution to this problem has a closed form that can be easily written as follows. Let $\{m_1, m_2, m_3\}$ be the scaled monomial basis of $\mathbb{P}_1(\mathbf{P})$, which is given by:

$$m_1(x, y) = 1, \quad m_2(x, y) = \frac{x - x_{\mathbf{P}}}{h_{\mathbf{P}}}, \quad \text{and} \quad m_3(x, y) = \frac{y - y_{\mathbf{P}}}{h_{\mathbf{P}}},$$

where $\mathbf{x}_P = (x_P, y_P)^T$ is the position vector of the barycenter of P . Let

$$\Pi_P^{LS} D_h(x, y) = am_1(x, y) + bm_2(x, y) + cm_3(x, y).$$

We denote the position vector of the i -th vertex \mathbf{v}_i by \mathbf{x}_i , for $i = 1, \dots, N$, where N is the number of vertices of P . Then, the coefficient vector $\boldsymbol{\xi} = (a, b, c)^T$ is the solution of the system

$$\mathbb{A}\boldsymbol{\xi} = \mathbf{b} \quad \text{with} \quad \mathbb{A} = \begin{pmatrix} m_1(\mathbf{x}_1) & m_2(\mathbf{x}_1) & m_3(\mathbf{x}_1) \\ m_1(\mathbf{x}_2) & m_2(\mathbf{x}_2) & m_3(\mathbf{x}_2) \\ \vdots & \vdots & \vdots \\ m_1(\mathbf{x}_N) & m_2(\mathbf{x}_N) & m_3(\mathbf{x}_N) \end{pmatrix}, \quad \mathbf{b} = \begin{pmatrix} D_h(\mathbf{x}_1) \\ D_h(\mathbf{x}_2) \\ \vdots \\ D_h(\mathbf{x}_N) \end{pmatrix}. \quad (40)$$

Since \mathbb{A} is a maximum rank matrix, the array of the solution coefficients is given by $\boldsymbol{\xi} = (\mathbb{A}^T \mathbb{A})^{-1} \mathbb{A}^T \mathbf{b}$.

(III) Galerkin Interpolation operator. The final projector that we consider in this chapter is denoted as Π_P^{pw} and is the piecewise linear Galerkin interpolation on a triangular partition of P . If P is a convex polygon, we can easily build such triangular partition by connecting its vertices and the barycenter given by the convex linear combination

$$\mathbf{x}_v^* = \sum_{v \in \partial P} \alpha_v \mathbf{x}_v,$$

for some suitable choices of the coefficients α_v that are such that $0 \leq \alpha_v \leq 1$ for every v and $\sum_{v \in \partial P} \alpha_v = 1$. If P is only star-shaped but not necessarily convex, we can still define an inner point \mathbf{v}^* by a different choice of the coefficients α_v . For a given function $D_h \in \mathcal{V}_h(P)$, we assume that

$$\Pi_P^{pw} D_h(\mathbf{x}_v^*) = \sum_{v \in \partial P} \alpha_v D_h(v) \quad \text{and} \quad \Pi_P^{pw} D_h(\mathbf{x}_v) = D_h(\mathbf{x}_v) \quad \forall v \in \partial P.$$

Then, in every triangle T with vertices $\mathbf{v}_1, \mathbf{v}_2$ and \mathbf{v}^* , we define $\Pi_P^{pw} D_h(\mathbf{x})$ as the linear interpolant of the values $D_h(\mathbf{v}_1), D_h(\mathbf{v}_2)$, and $D_h(\mathbf{v}^*)$.

3.3. The Edge Space

The next virtual element space that we consider is the finite dimensional counterpart of $H(\text{div}; \Omega)$. This space was introduced in [9]. Like before, we begin by defining a local space over a cell P . The formal definition reads as

$$\mathcal{E}_h(P) := \left\{ \mathbf{C}_h \in H(\text{div}; P) \cap H(\text{rot}; P) : \text{div } \mathbf{C}_h \in \mathbb{P}_0(P), \text{ rot } \mathbf{C}_h = 0, \right. \\ \left. \mathbf{C}_h|_e \cdot \mathbf{n} \in \mathbb{P}_0(e) \quad \forall e \in \partial P \right\}. \quad (41)$$

Every virtual element function $\mathbf{C}_h \in \mathcal{E}_h(P)$ is characterized by the following set of degrees of freedom

(E) the average of the normal flux on each edge:

$$\forall e \in \partial P : \quad \frac{1}{|e|} \int_e \mathbf{C}_h \cdot \mathbf{n} \, dl.$$

These are represented by red arrows pointing out the edges of the cell P , see the sample picture in Figure 2.

In order to properly state the property of unisolvency we introduce $\mathcal{R}_e : H(\text{div}; P) \rightarrow \mathbb{R}^N$ such that for any $\mathbf{C} \in H(\text{div}; P)$ the array $\mathcal{R}_e(\mathbf{C})$ is the array of degrees of freedom of \mathbf{C} . This result is stated below

Theorem 3.5 *Let $\mathcal{K}_e : \mathcal{E}_h(P) \rightarrow \mathbb{R}^N$ be the restriction of \mathcal{R}_e . Then, \mathcal{K}_e is bijective.*

In view of the unisolvency of $\mathcal{E}_h(P)$, we define the interpolation operator $\mathcal{I}_P^{\mathcal{E}_h} = \mathcal{K}_e^{-1} \circ \mathcal{R}_e$.

Next, we define an important projector in the space $\mathcal{E}_h(P)$, namely the orthogonal projections $\Pi_P^0 : \mathcal{E}_h(P) \rightarrow \mathbb{P}_0(P)$ whose image are the solution to the variational problem

$$(\mathbf{C}_h - \Pi_P^0 \mathbf{C}_h, \mathbf{q})_P = 0 \quad \text{for all} \quad \mathbf{q} \in [\mathbb{P}_0(P)]^2, \quad (42)$$

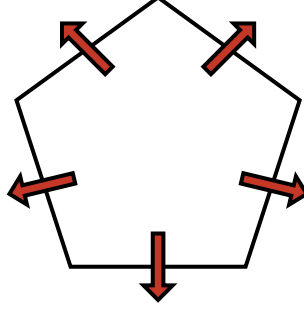


Fig. 2. Representation of the degrees of freedom of functions in $\mathcal{E}_h(\mathbf{P})$.

for every $\mathbf{C}_h \in \mathcal{E}_h(\mathbf{P})$, and where $\text{RT}_0(\mathbf{P})$ is the space of vector-valued functions over \mathbf{P} defined as This projector are computable using the degrees of freedom (\mathbf{E}) . Pick $\mathbf{q} \in [\mathbb{P}_0(\mathbf{P})]^2$, $p \in \mathbb{P}_1(\mathbf{P})$ where the scalar polynomial p is chosen so that $\mathbf{q} = \nabla p$. Then, we apply the Green theorem and we find that

$$\int_{\mathbf{P}} \mathbf{C}_h \cdot \mathbf{q} \, dA = \int_{\mathbf{P}} \mathbf{C}_h \cdot \nabla p \, dA = - \int_{\mathbf{P}} (\text{div } \mathbf{C}_h) p \, dA + \int_{\partial \mathbf{P}} p \mathbf{C}_h \cdot \mathbf{n} \, d\ell \quad (43)$$

for all $\mathbf{C}_h \in \mathcal{E}_h(\mathbf{P})$. We split the integral on $\partial \mathbf{P}$ in the summation of line integrals

$$\int_{\partial \mathbf{P}} \mathbf{C}_h \cdot \mathbf{n} p \, d\ell = \sum_{\mathbf{e} \in \partial \mathbf{P}} (\mathbf{C}_h \cdot \mathbf{n})|_{\mathbf{e}} \int_{\mathbf{e}} p \, d\ell, \quad (44)$$

and we note that $\mathbf{C}_h \cdot \mathbf{n}|_{\mathbf{e}}$ is constant on each edge $\mathbf{e} \in \partial \mathbf{P}$, cf. space definition (41), and coincides with the evaluation in (\mathbf{E}) . In turn, we compute $\text{div } \mathbf{C}_h \in \mathbb{P}_0(\mathbf{P})$ by applying the divergence theorem:

$$\text{div } \mathbf{C}_h = \frac{1}{|\mathbf{P}|} \int_{\partial \mathbf{P}} \mathbf{C}_h \cdot \mathbf{n} \, d\ell = \frac{1}{|\mathbf{P}|} \sum_{\mathbf{e} \in \partial \mathbf{P}} |\mathbf{e}| \left(\frac{1}{|\mathbf{e}|} \int_{\mathbf{e}} \mathbf{C}_h \cdot \mathbf{n} \, d\ell \right). \quad (45)$$

Note that the polynomial p is determined by the relation $\nabla p = \mathbf{q}$ and is defined up to an additive constant factor. If we choose this constant factor equal to the elemental average of p on \mathbf{P} , so that $\int_{\mathbf{P}} p \, dA = 0$, we can make the area integral vanish since

$$\int_{\mathbf{P}} (\text{div } \mathbf{C}_h) p \, dA = (\text{div } \mathbf{C}_h)|_{\mathbf{P}} \int_{\mathbf{P}} p \, dA = 0. \quad (46)$$

In conclusion, the information about a virtual element function \mathbf{C}_h in the space $\mathcal{E}_h(\mathbf{P})$ that we need to compute the projection $\Pi_{\mathbf{P}}^0 \mathbf{C}_h$ can be read off the degrees of freedom of \mathbf{C}_h .

We can use $\Pi_{\mathbf{P}}^0$ to define the inner product:

$$(\mathbf{B}_h, \mathbf{C}_h)_{\mathcal{E}_h(\mathbf{P})} = (\Pi_{\mathbf{P}}^0 \mathbf{B}_h, \Pi_{\mathbf{P}}^0 \mathbf{C}_h) + \mathcal{S}^e((\mathcal{I} - \Pi_{\mathbf{P}}^0) \mathbf{B}_h, (\mathcal{I} - \Pi_{\mathbf{P}}^0) \mathbf{C}_h) \quad (47)$$

for every possible pair of virtual element functions $\mathbf{B}_h, \mathbf{C}_h \in \mathcal{E}_h(\mathbf{P})$. As before, the stabilization form \mathcal{S}^e can be any continuous bilinear form for which there exists two strictly positive constants s_* and s^* independent of h such that

$$s_* \|\mathbf{C}_h\|_{0,\mathbf{P}}^2 \leq \mathcal{S}^e(\mathbf{C}_h, \mathbf{C}_h) \leq s^* \|\mathbf{C}_h\|_{0,\mathbf{P}}^2 \quad \forall \mathbf{C}_h \in \mathcal{E}_h(\mathbf{P}) \cap \ker \Pi_{\mathbf{P}}^0 \cap \mathcal{E}_h(\mathbf{P}).$$

Practical implementations of \mathcal{S}^e can be designed according with [57, 37] for more examples. The constants s_* and s^* are different from those in equation (28). This inner product defines the norm

$$\|\mathbf{C}_h\|_{\mathcal{E}_h(\mathbf{P})} = (\mathbf{C}_h, \mathbf{C}_h)_{\mathcal{E}_h(\mathbf{P})}^{1/2} \quad \forall \mathbf{C}_h \in \mathcal{E}_h(\mathbf{P}), \quad (48)$$

and the two fundamental properties of \mathbb{P}_0 -consistency and stability hold as stated in the following theorem.

Theorem 3.6 *The inner product $(\cdot, \cdot)_{\mathcal{E}_h(\mathbf{P})}$ defined in (47) has the two properties:*

– \mathbb{P}_0 -consistency:

$$(\mathbf{C}_h, \mathbf{q})_{\mathcal{E}_h(\mathbf{P})} = (\mathbf{C}_h, \mathbf{q}) \quad \forall \mathbf{C}_h \in \mathcal{E}_h(\mathbf{P}), \mathbf{q} \in [\mathbb{P}_0(\mathbf{P})]^2 \quad (49)$$

– **Stability:** there exists two real constants β_* and $\beta^* > 0$ independent of h and P such that

$$\beta_* \|C_h\|_{0,P}^2 \leq \|C_h\|_{\mathcal{E}_h(P)}^2 \leq \beta^* \|C_h\|_{0,P}^2 \quad \forall C_h \in \mathcal{E}_h(P). \quad (50)$$

Proof 1 We omit the proof of this Theorem since it is essentially the same as the one presented for Theorem 3.3. We just note that here the orthogonality of the projector $\Pi_P^0 P$ makes a more general result possible as the consistency condition is verified if at least one and not necessarily both of the entries of $(C_h, q)_{\mathcal{E}_h(P)}$ is a (vector-valued) polynomial field. In fact, if $q \in [\mathbb{P}_2(P)]^2$ we have that $\mathcal{S}^e((\mathcal{I} - \Pi_P^0)C_h, (\mathcal{I} - \Pi_P^0)q) = 0$ because $\Pi_P^0 q = q$. Then, the definition of the orthogonal projection Π_P^0 , which is also polynomial-preserving, implies that

$$(B_h, C_h)_{\mathcal{E}_h(P)} = (\Pi_P^0 C_h, \Pi_P^0 q)_P = (C_h, \Pi_P^0 q)_P = (C_h, q)_P \quad (51)$$

for all $C_h \in \mathcal{E}_h(P)$ and $q \in \mathbb{P}_0(P)$.

We introduce the global virtual element space \mathcal{E}_h built on the mesh Ω_h by pasting together the elemental spaces $\mathcal{E}_h(P)$ built on all cells P :

$$\mathcal{E}_h = \{C_h \in H(\text{div}; \Omega) : C_h|_P \in \mathcal{E}_h(P) \quad \forall P \in \Omega_h\}.$$

We endow this space with the inner product

$$(B_h, C_h)_{\mathcal{E}_h} = \sum_{P \in \Omega_h} (B_h|_P, C_h|_P)_{\mathcal{E}_h(P)} \quad \forall B_h, C_h \in \mathcal{E}_h, \quad (52)$$

and the induced norm

$$\|C_h\|_{\mathcal{E}_h}^2 = (C_h, C_h)_{\mathcal{E}_h} \quad \forall C_h \in \mathcal{E}_h. \quad (53)$$

As for the nodal space, this global inner product and associated norm satisfy the fundamental properties of \mathbb{P}_0 -consistency and stability, which we state in the next corollary. These properties imply the exactness of the inner product defined in (52) on the piecewise constant functions and that the norm defined in (47) is equivalent to the L^2 norm. We omit the proof since these properties are an immediate consequence of Theorem 3.6.

Corollary 3.7 The inner product $(\cdot, \cdot)_{\mathcal{E}_h}$ defined in (52) has the two properties:

– **Linear consistency:**

$$(C_h, q)_{\mathcal{E}_h(P)} = (C_h, q) \quad \forall C_h \in \mathcal{E}_h, q \in [\mathbb{P}_0(\Omega_h)]^2. \quad (54)$$

– **Stability:** there exists two real constants β_* and $\beta^* > 0$ independent of h such that

$$\beta_* \|C_h\|_{0,P}^2 \leq \|C_h\|_{\mathcal{E}_h(P)}^2 \leq \beta^* \|C_h\|_{0,P}^2 \quad \forall C_h \in \mathcal{E}_h(P). \quad (55)$$

Next, we introduce the global interpolation operator $\mathcal{I}_P^{\mathcal{E}_h} : H(\text{div}; \Omega) \rightarrow \mathcal{V}_h$. This operator is defined by gluing together its respective elemental definitions, so that

$$\mathcal{I}^{\mathcal{E}_h}(C_h)|_P = \mathcal{I}_P^{\mathcal{E}_h}(C_h|_P)$$

To end this subsection we will define a second orthogonal projection that we will use to approximate a term unique to MHD. Consider a cell P and define $\Pi_P^{RT} : \mathcal{E}_h(P) \rightarrow \text{RT}_0(P)$. Given $C_h \in \mathcal{E}_h(P)$ the image $\Pi_P^{RT} C_h$ is the solution to the variational formulation

$$(C_h - \Pi_P^{RT} C_h, q)_P = 0 \quad \text{for all } q \in \text{RT}_0(P), \quad (56)$$

where

$$\text{RT}_0(P) = \left\{ a \begin{pmatrix} 1 \\ 0 \end{pmatrix} + b \begin{pmatrix} 0 \\ 1 \end{pmatrix} + c \begin{pmatrix} x \\ y \end{pmatrix} : a, b, c \in \mathbb{R} \right\}.$$

This projector is also computable using only the degrees of freedom in $\mathcal{E}_h(P)$. The strategy is the same as the one presented for Π_P^0 . Consider $q \in \text{RT}_0(P)$ and $p \in \mathbb{P}_2(P)$ with $\int_P p dA = 0$ such that $\nabla p = q$. The terms in Green's Theorem (43) can be computed as before with the only difference being that the quadrature rule used in (44) needs to be exact for quadratic polynomials.

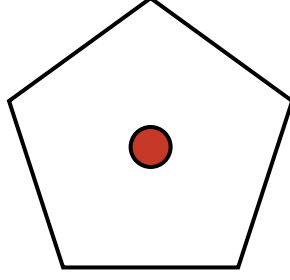


Fig. 3. Representation of the degrees of freedom of functions in $\mathcal{P}_h(\mathbf{P})$.

The *global orthogonal projector* $\Pi^{RT} : \mathcal{E}_h \rightarrow \text{RT}_0(\Omega_h)$, where $\text{RT}_0(\Omega_h) = \{\mathbf{q} \in H(\text{div}; \Omega) : \mathbf{q}|_{\mathbf{P}} \in \text{RT}_0(\mathbf{P})\}$ is defined as

$$(\Pi^{RT} \mathbf{C}_h)|_{\mathbf{P}} = \Pi_{\mathbf{P}}^{RT}(\mathbf{C}_h|_{\mathbf{P}}) \quad \forall \mathbf{P} \in \Omega_h. \quad (57)$$

We use Π^{RT} to approximate the term " $\mathbf{u} \times \mathbf{B}$ " as can be evidenced in the MHD variational formulation (20). The main issue with the aforementioned term is that we only have access to the fluxes of the magnetic field across the edges while the inner product in the variational formulation requires nodal evaluations. We amend this inconsistency by projecting the magnetic field onto the space of vector polynomial fields $\text{RT}_0(\mathbf{P})$ and extract the necessary evaluations from this projection. We note that we could use $\Pi_{\mathbf{P}}^0$ to extract these vertex evaluations. However, more complex MHD models have terms of the form

$$((\text{rot } \mathbf{B}) \times \mathbf{B}, D). \quad (58)$$

Such a quantity cannot be estimated using $\Pi_{\mathbf{P}}^0$ since the codomain of this projector is the space of constants and their curl is zero. In this case using the projector Π^{RT} is ideal for low order approximations.

3.4. The cell space

The final space that we need to define for the electromagnetic part is the space of piecewise constant functions on Ω_h , i.e., the space of constant polynomials in every element \mathbf{P} :

$$\mathcal{P}_h = \{q_h \in L^2(\Omega) : q_h|_{\mathbf{P}} \in \mathbb{P}_0(\mathbf{P}) \quad \forall \mathbf{P} \in \Omega_h\}. \quad (59)$$

The degrees of freedom of a function $q_h \in \mathcal{P}_h$ are given by

(D) the elemental averages of q_h over every cell $\mathbf{P} \in \Omega_h$

$$\frac{1}{|\mathbf{P}|} \int_{\mathbf{P}} q_h \, dA. \quad (60)$$

These are represented by red disks in the interior of the cell \mathbf{P} , see the sample picture in Figure 3. It is straightforward to see that such degrees of freedom are unisolvent in \mathcal{P}_h . In fact, the constant value given by restricting a function q_h to a cell is precisely the degree of freedom of q_h associated with that cell. We endow the elemental space \mathcal{P}_h with the inner product

$$(p_h, q_h)_{\mathcal{P}_h} = \sum_{|\mathbf{P}|} |\mathbf{P}| p_h|_{\mathbf{P}} q_h|_{\mathbf{P}} \quad \forall p_h, q_h \in \mathcal{P}_h,$$

which is the $L^2(\Omega)$ inner product of two piecewise constant functions. This inner product induces the norm

$$\|q_h\|_{\mathcal{P}_h}^2 = (q_h, q_h)_{\mathcal{P}_h}, \quad \forall q_h \in \mathcal{P}_h,$$

which is the $L^2(\Omega)$ -norm restricted to the functions of \mathcal{P}_h , so that

$$\|q_h\|_{\mathcal{P}_h} = \|q_h\|_{0,\Omega} \quad \forall q_h \in \mathcal{P}_h.$$

Finally, we define the *global interpolation operator* $\mathcal{I}^{\mathcal{P}_h} : L^2(\Omega) \rightarrow \mathcal{P}_h$ such that for every $q \in L^2(\Omega)$ we have:

$$(\mathcal{I}^{\mathcal{P}_h} q)|_{\mathbf{P}} = \frac{1}{|\mathbf{P}|} \int_{\mathbf{P}} q \, dA \quad \forall \mathbf{P} \in \Omega_h. \quad (61)$$

3.5. The de Rham complex.

In the previous sections we introduced and discussed the virtual element spaces \mathcal{V}_h , \mathcal{E}_h and \mathcal{P}_h . It is well-known that the spaces $H(\mathbf{rot}; \Omega)$, $H(\text{div}; \Omega)$ and $L^2(\Omega)$ form the de Rham chain

$$H(\mathbf{rot}; \Omega) \xrightarrow{\mathbf{rot}} H(\text{div}; \Omega) \xrightarrow{\text{div}} L^2(\Omega). \quad (62)$$

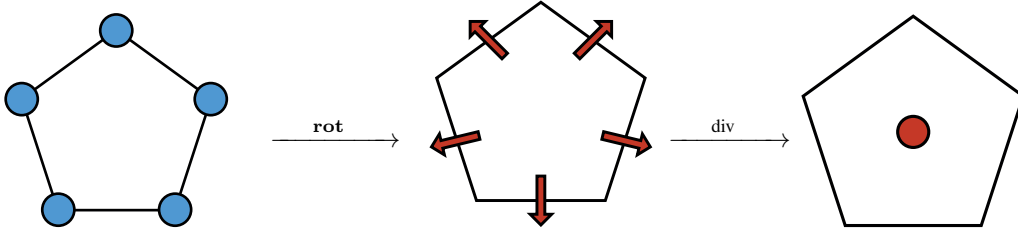
If Ω is simply connected, the chain is exact, see [61]. Equivalently, we can say that

$$\mathbf{rot} H(\mathbf{rot}; \Omega) = \{ \mathbf{C} \in H(\text{div}; \Omega) : \text{div } \mathbf{C} = 0 \}.$$

In the spirit of constructing a discrete version of the continuous problem, the spaces \mathcal{V}_h , \mathcal{E}_h and \mathcal{P}_h also form a similar exact de Rham chain

$$\mathcal{V}_h \xrightarrow{\mathbf{rot}} \mathcal{E}_h \xrightarrow{\text{div}} \mathcal{P}_h. \quad (63)$$

This chain was first introduced in [7], and explored in more details and generality in [9]. It reveals that the set of degrees of freedom are transformed in accordance with the following diagram:



First we want to show that the chain in (63) is well-defined. This is to say that two important inclusions hold. The first is presented in the following lemma.

Lemma 3.8 *Let \mathcal{V}_h and \mathcal{E}_h be the virtual element spaces defined in (25) and (41) respectively. Then, it holds that*

$$\mathbf{rot} \mathcal{V}_h \subset \mathcal{E}_h. \quad (64)$$

Proof. Let \mathbf{P} be a mesh cell of Ω_h and take $D_h \in \mathcal{V}_h(\mathbf{P})$. In view of the definition of $\mathcal{V}_h(\mathbf{P})$, we have that $\mathbf{rot} \mathbf{rot} D_h = 0$ in \mathbf{P} and, clearly, $\text{div } \mathbf{rot} D_h = 0 \in \mathbb{P}_0(\mathbf{P})$. Moreover, for every edge $\mathbf{e} \in \partial \mathbf{P}$, we find that $(\mathbf{rot} D_h \cdot \mathbf{n})|_{\mathbf{e}} = (\nabla D_h \cdot \mathbf{t})|_{\mathbf{e}} \in \mathbb{P}_0(\mathbf{e})$. Consequently, $(\mathbf{rot} D_h)|_{\mathbf{P}} \in \mathcal{E}_h(\mathbf{P})$, and, thus, $\mathbf{rot} D_h \in \mathcal{E}_h$ for every $D_h \in \mathcal{V}_h$ proving the inclusion relation in (64). \square

From Lemma 3.8, we know that $\mathbf{rot} D_h \in \mathcal{E}_h$ if $D_h \in \mathcal{V}_h$. Moreover, we can compute the degrees of freedom of $\mathbf{rot} D_h$ in \mathcal{E}_h from the degrees of freedom of D_h in \mathcal{V}_h . In fact, by applying the fundamental theorem of line integrals, we find that

$$\frac{1}{|\mathbf{e}|} \int_{\mathbf{e}} \mathbf{rot} D_h \cdot \mathbf{n} \, d\ell = \frac{1}{|\mathbf{e}|} \int_{\mathbf{e}} \nabla D_h \cdot \mathbf{t} \, d\ell = \frac{D_h(\mathbf{v}_2) - D_h(\mathbf{v}_1)}{|\mathbf{e}|}, \quad (65)$$

for every edge \mathbf{e} of the polygonal boundary $\partial \mathbf{P}$ with endpoints \mathbf{v}_1 and \mathbf{v}_2 (oriented from \mathbf{v}_1 to \mathbf{v}_2), where again we used the identity $\mathbf{n} \cdot \mathbf{rot} (D_h) = \mathbf{t} \cdot \nabla (D_h)$. In view of equation (65), we can read the necessary information to identify the image of the rotational of \mathcal{V}_h as a subset of \mathcal{E}_h by using the degrees of freedom defined for \mathcal{V}_h .

The second inclusion in the chain (63) is the conclusion of the following lemma.

Lemma 3.9 *Let \mathcal{E}_h and \mathcal{P}_h be the virtual element spaces defined in (41), and (59). Then, it holds that*

$$\text{div } \mathcal{E}_h \subset \mathcal{P}_h. \quad (66)$$

Proof. To verify this inclusion, we only need to note that any $\mathbf{C}_h \in \mathcal{E}_h(\mathbf{P})$ is such that $\text{div } \mathbf{C}_h \in \mathbb{P}_0(\mathbf{P})$ from the definition of $\mathcal{E}_h(\mathbf{P})$. It follows that $\text{div } \mathbf{C}_h \in \mathbb{P}_0(\Omega_h) = \mathcal{P}_h$ for every $\mathbf{C}_h \in \mathcal{E}_h$, which is the second inclusion relation in (66). \square

Noting that the divergence of a function in \mathcal{E}_h lies in \mathcal{P}_h will help us identify that its divergence can be entirely characterized by its set of degrees of freedom in \mathcal{P}_h . Take $\mathbf{C}_h \in \mathcal{E}_h$. From the divergence theorem we have that

$$\frac{1}{|\mathbf{P}|} \int_{\mathbf{P}} \operatorname{div} \mathbf{C}_h dA = \frac{1}{|\mathbf{P}|} \int_{\partial \mathbf{P}} \operatorname{div} \mathbf{C}_h dA = \frac{1}{|\mathbf{P}|} \sum_{\mathbf{e} \in \partial \mathbf{P}} |\mathbf{e}| \left(\frac{1}{|\mathbf{e}|} \int_{\mathbf{e}} \mathbf{C}_h \cdot \mathbf{n} dA \right). \quad (67)$$

Hence, we can evaluate the divergence of a function $\mathbf{C}_h \in \mathcal{E}_h$ using only its degrees of freedom.

The results summarized by equations (65) and (67) are essential in order to further study the spaces $\mathcal{V}_h, \mathcal{E}_h$ and \mathcal{P}_h and their relationship with the larger spaces $H(\mathbf{rot}; \Omega), H(\operatorname{div}; \Omega)$ and $L^2(\Omega)$. These spaces form the commutative diagram

$$\begin{array}{ccccc} H(\mathbf{rot}; \Omega) & \xrightarrow{\mathbf{rot}} & H(\operatorname{div}; \Omega) & \xrightarrow{\operatorname{div}} & L^2(\Omega) \\ \downarrow \mathcal{I}^{\mathcal{V}_h} & & \downarrow \mathcal{I}^{\mathcal{E}_h} & & \downarrow \mathcal{I}^{\mathcal{P}_h} \\ \mathcal{V}_h & \xrightarrow{\mathbf{rot}} & \mathcal{E}_h & \xrightarrow{\operatorname{div}} & \mathcal{P}_h \end{array} \quad (68)$$

The proof of this theorem is broken into two lemmas. The first lemma, presented below, involves the spaces $H(\mathbf{rot}; \Omega)$ and $H(\operatorname{div}; \Omega)$, and their discrete counterparts \mathcal{V}_h and \mathcal{E}_h .

Lemma 3.10 *The following identity holds*

$$\forall D \in H(\mathbf{rot}; \Omega) : \quad \mathcal{I}^{\mathcal{E}_h} \circ \mathbf{rot}(D) = \mathbf{rot} \circ \mathcal{I}^{\mathcal{V}_h}(D), \quad (69)$$

i.e., the interpolation and the rotational operators commute.

Proof. Take a scalar function $D \in H(\mathbf{rot}; \Omega)$. By definition, the degrees of freedom of $\mathcal{I}^{\mathcal{E}_h} \circ \mathbf{rot}(D)$ in \mathcal{E}_h are the same of $\mathbf{rot} D$. So, if \mathbf{e} is a mesh edge oriented from endpoint \mathbf{v}_1 to \mathbf{v}_2 , the theorem of line integral yields:

$$\frac{1}{|\mathbf{e}|} \int_{\mathbf{e}} \mathbf{n} \cdot \mathbf{rot} D d\ell = \frac{1}{|\mathbf{e}|} \int_{\mathbf{e}} \mathbf{t} \cdot \nabla D d\ell = \frac{D(\mathbf{v}_2) - D(\mathbf{v}_1)}{|\mathbf{e}|}. \quad (70)$$

In turn, the degrees of freedom of $\mathbf{rot} \circ \mathcal{I}^{\mathcal{V}_h}(D)$ are given by

$$\frac{1}{|\mathbf{e}|} \int_{\mathbf{e}} \mathbf{n} \cdot \mathbf{rot} (\mathcal{I}^{\mathcal{V}_h}(D)) d\ell = \frac{1}{|\mathbf{e}|} \int_{\mathbf{e}} \mathbf{t} \cdot \nabla \mathcal{I}^{\mathcal{V}_h}(D) d\ell = \frac{\mathcal{I}^{\mathcal{V}_h} D(\mathbf{v}_2) - \mathcal{I}^{\mathcal{V}_h} D(\mathbf{v}_1)}{|\mathbf{e}|}, \quad (71)$$

using again the theorem of line integral yields. The definition of operator $\mathcal{I}^{\mathcal{V}_h}$ is such that

$$\mathcal{I}^{\mathcal{V}_h} D(\mathbf{v}_1) = D(\mathbf{v}_1) \quad \text{and} \quad \mathcal{I}^{\mathcal{V}_h} D(\mathbf{v}_2) = D(\mathbf{v}_2).$$

Thus, equations (70) and (71) imply that the functions $\mathcal{I}^{\mathcal{E}_h} \circ \mathbf{rot}(D)$ and $\mathbf{rot} \circ \mathcal{I}^{\mathcal{V}_h}(D)$ have the same degrees of freedom in \mathcal{E}_h and relation (69) follows from the unisolvence. \square

The second lemma involves the spaces $H(\operatorname{div}; \Omega), L^2(\Omega), \mathcal{E}_h$ and \mathcal{P}_h .

Lemma 3.11 *The following identity holds*

$$\forall \mathbf{C} \in H(\operatorname{div}; \Omega) : \quad \mathcal{I}^{\mathcal{P}_h} \circ \operatorname{div}(\mathbf{C}) = \operatorname{div} \circ \mathcal{I}^{\mathcal{E}_h}(\mathbf{C}), \quad (72)$$

i.e., the interpolation and the divergence operators commute.

Proof 2 We prove (72) by verifying that the two functions in the left and right side share the same degrees of freedom in \mathcal{P}_h . Take a vector-valued field $\mathbf{C} \in H(\operatorname{div}; \Omega)$. By definition, the degrees of freedom of $\mathcal{I}^{\mathcal{P}_h} \circ \operatorname{div}(\mathbf{C})$ in \mathcal{E}_h are the same of $\operatorname{div}(\mathbf{C})$. So, if \mathbf{P} is a mesh cell, the divergence theorem yields

$$\frac{1}{|\mathbf{P}|} \int_{\mathbf{P}} \operatorname{div} \mathbf{C} dA = \frac{1}{|\mathbf{P}|} \sum_{\mathbf{e} \in \partial \mathbf{P}} \int_{\mathbf{e}} \mathbf{C} \cdot \mathbf{n} d\ell. \quad (73)$$

In turn, the degrees of freedom of $\operatorname{div} \circ \mathcal{I}^{\mathcal{E}_h}(\mathbf{C})$ are given by

$$\frac{1}{|\mathbf{P}|} \int_{\mathbf{P}} \operatorname{div} \mathcal{I}^{\mathcal{E}_h}(\mathbf{C}) dA = \frac{1}{|\mathbf{P}|} \sum_{\mathbf{e} \in \partial \mathbf{P}} \int_{\mathbf{e}} \mathcal{I}^{\mathcal{E}_h}(\mathbf{C}) \cdot \mathbf{n} d\ell. \quad (74)$$

The definition of operator $\mathcal{I}^{\mathcal{E}_h}$ is such that

$$\forall \mathbf{e} \in \partial \mathbf{P}: \int_{\mathbf{e}} \mathcal{I}^{\mathcal{E}_h} \mathbf{C} \cdot \mathbf{n} \, d\ell = \int_{\mathbf{e}} \mathbf{C} \cdot \mathbf{n} \, d\ell.$$

Thus, equations (73) and (74) imply that the two functions $\mathcal{I}^{\mathcal{P}_h} \circ \operatorname{div}(\mathbf{C})$ and $\operatorname{div} \circ \mathcal{I}^{\mathcal{E}_h}(\mathbf{C})$ have the same degrees of freedom in \mathcal{P}_h and relation (72) follows from the unisolvence.

We summarize our findings in the following theorem

Theorem 3.12 *The chain in (63) is well-defined and exact, and diagram (68) is commutative.*

Proof 3 *Lemmas 3.8 and 3.9 prove that (63) is well-defined. Lemmas 3.10 and 3.11 prove that diagram (68) is commutative. Hence, we are only left to prove that the de Rham chain (63) is exact, or, equivalently that*

$$\operatorname{rot} \mathcal{V}_h = \ker(\operatorname{div} \mathcal{E}_h) = \{\mathbf{C}_h \in \mathcal{E}_h : \operatorname{div} \mathbf{C}_h = 0\}. \quad (75)$$

Take $D_h \in \mathcal{V}_h$. Lemma 3.8 implies that $\operatorname{rot} D_h \in \mathcal{E}_h$, and, obviously, $\operatorname{div} \operatorname{rot} D_h = 0$, so that $\operatorname{rot} D_h \in \ker(\operatorname{div} \mathcal{E}_h)$ as defined in (75), which implies that $\operatorname{rot} \mathcal{V}_h \subseteq \ker(\operatorname{div} \mathcal{E}_h)$. Next, consider $\mathbf{C}_h \in \mathcal{E}_h$ with $\operatorname{div} \mathbf{C}_h = 0$. Since $\mathcal{E}_h \subset H(\operatorname{div}; \Omega)$, then $\mathbf{C}_h \in H(\operatorname{div}; \Omega)$ and the exactness of chain (62) implies the existence of a scalar function $D \in H(\operatorname{rot}; \cdot)$ such that $\mathbf{C}_h = \operatorname{rot} D$. Moreover, $\mathcal{I}^{\mathcal{V}_h} D \in \mathcal{V}_h$ must verify

$$\operatorname{rot} \circ \mathcal{I}^{\mathcal{V}_h} D = \mathcal{I}^{\mathcal{E}_h} \circ \operatorname{rot} D = \mathcal{I}^{\mathcal{E}_h} \mathbf{C}_h = \mathbf{C}_h, \quad (76)$$

which implies that \mathbf{C}_h is the rotational of a function of \mathcal{V}_h and, thus, $\ker(\operatorname{div} \mathcal{E}_h) \subset \operatorname{rot} \mathcal{V}_h$.

3.6. Fluid Flow

In this section, we briefly review the virtual element spaces for the discretization of the fluid-flow equations in the MHD model. These spaces were originally proposed in [68, 15, 16].

The first virtual element space is used to discretize the pressure. We consider a subspace of \mathcal{P}_h as defined in Section 3.4. This subspace is given by

$$\mathcal{P}_{h,0} = \left\{ q_h \in \mathcal{P}_h : \int_{\Omega} q_h \, dA = 0 \right\}. \quad (77)$$

The degrees of freedom of a function $q_h \in \mathcal{P}_{h,0}$ are given by

$$(\mathbf{P}') \quad \int_{\mathbf{P}} q_h \, dA \quad \text{for every } \mathbf{P} \in \Omega_h.$$

These degrees of freedom are the same of \mathcal{P}_h up to a multiplicative scale factor equal to $1/|\mathbf{P}|$. For $\mathcal{P}_{h,0}$ we prefer this definition because the integral over $\mathcal{P}_{h,0}$ of a function $q_h \in \mathcal{P}_{h,0}$ is given by summing the degrees of freedom of q_h :

$$\int_{\Omega} q_h \, dA = \sum_{i=0}^N \operatorname{dof}_i(q_h).$$

If we enumerate the cells in the mesh Ω_h as $\{P_i : 1 \leq i \leq N\}$ then the functions $\operatorname{dof}_i : \mathcal{P}_{h,0} \rightarrow \mathbb{R}$ map each function in $\mathcal{P}_{h,0}$ to the degree of freedom associated with P_i .

The virtual element space for the velocity approximation reads as

$$\begin{aligned} \mathbf{V}_h(\mathbf{P}) = \left\{ \mathbf{v}_h \in [H^1(\mathbf{P})]^2 : \mathbf{v}_h|_{\partial \mathbf{P}} \in [\mathbb{B}(\partial \mathbf{P})]^2, \operatorname{div} \mathbf{v}_h \in \mathbb{P}_0(\mathbf{P}), \right. \\ \left. - \Delta \mathbf{v}_h - \nabla s = \mathbf{0} \text{ for some } s \in L_0^2(\mathbf{P}) \right\}, \end{aligned} \quad (78a)$$

where

$$\mathbb{B}(\partial \mathbf{P}) = \left\{ v \in C^0(\partial \mathbf{P}) : v|_{\mathbf{e}} \in \mathbb{P}_2(\mathbf{e}) \, \forall \mathbf{e} \in \partial \mathbf{P} \right\}. \quad (78b)$$

A function $\mathbf{v}_h \in \mathbf{V}_h(\mathbf{P})$ is uniquely characterized by the following degrees of freedom:

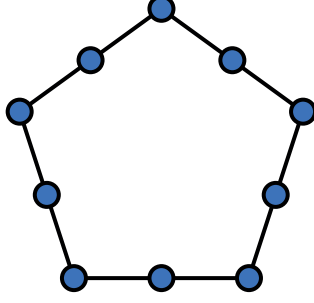


Fig. 4. Representation of the degrees of freedom of functions in $\mathbf{V}_h(\mathbf{P})$.

(D1) pointwise evaluations of \mathbf{v}_h at the vertices of \mathbf{P} ;

(D2) pointwise evaluations at \mathbf{v}_h at the midpoint of the edges of $\partial\mathbf{P}$.

These are represented by blue disks centered at the nodes and the mid-point of edges of the cell \mathbf{P} , see the sample picture in Figure 4.

Theorem 3.13 Define the map $\mathcal{K}_{\mathbf{V}_h} : \mathbf{V}_h(\mathbf{P}) \rightarrow \mathbb{R}^N$ such that for any $\mathbf{v}_h \in \mathbf{V}_h(\mathbf{P})$ the array $\mathcal{K}_{\mathbf{V}_h} \mathbf{v}_h$ is given by the degrees of freedom of \mathbf{v}_h . Then, $\mathcal{K}_{\mathbf{V}_h}$ is bijective.

Proof. The proof is omitted and can be found in [15]. \square

The largest polynomial space that is contained in $\mathbf{V}_h(\mathbf{P})$ is the space of divergence-free, quadratic polynomial vectors, which is formally written as:

$$\mathbf{P}(\mathbf{P}) = \left\{ \mathbf{q} \in [\mathbb{P}_2(\mathbf{P})]^2 : \operatorname{div} \mathbf{q} \in \mathbb{P}_0(\mathbf{P}) \right\}.$$

Let $\mathcal{E}_{\mathbf{P}}$ denote the set of vertices and midpoints of the edges forming the polygonal boundary $\partial\mathbf{P}$, and consider the projector $\Pi_{\mathbf{P}}^{\nabla} : \mathbf{V}_h(\mathbf{P}) \rightarrow \mathbf{P}(\mathbf{P})$ such that the vector polynomial $\Pi_{\mathbf{P}}^{\nabla} \mathbf{v}_h$ for $\mathbf{v}_h \in \mathbf{V}_h(\mathbf{P})$ is the solution to the following variational problem

$$\int_{\mathbf{P}} \nabla \Pi_{\mathbf{P}}^{\nabla} \mathbf{v}_h : \nabla \mathbf{q} \, dA = \int_{\mathbf{P}} \nabla \mathbf{v}_h : \nabla \mathbf{q} \, dA \quad \forall \mathbf{q} \in \mathbf{P}(\mathbf{P}), \quad (79a)$$

$$P_0(\Pi_{\mathbf{P}}^{\nabla} \mathbf{v}_h) = P_0(\mathbf{v}_h), \quad (79b)$$

where

$$P_0(\mathbf{v}_h) = \sum_{\mathbf{v} \in \mathcal{E}_{\mathbf{P}}} \mathbf{v}_h(\mathbf{v}). \quad (80)$$

We recall that $\nabla \mathbf{v}_h$, $\nabla \Pi_{\mathbf{P}}^{\nabla} \mathbf{v}_h$ and $\nabla \mathbf{q}$ are 2×2 -sized tensors and “ \cdot ” is the usual euclidean scalar product saturating both indices of such tensors, so that

$$\nabla \mathbf{v} : \nabla \mathbf{w} = \sum_{i,j} (\partial v_i / \partial x_j) (\partial w_i / \partial x_j). \quad (81)$$

To prove that this projection operator is computable, we need to show that the right-hand side of (79a) is computable for every vector-valued field $\mathbf{v}_h \in \mathbf{V}_h(\mathbf{P})$ and $\mathbf{q} \in \mathbf{P}(\mathbf{P})$ using only the degrees of freedom of \mathbf{v}_h . To this end, we first apply the Green theorem to find that

$$\int_{\mathbf{P}} \nabla \mathbf{v}_h : \nabla \mathbf{q} \, dA = \int_{\partial\mathbf{P}} \mathbf{v}_h \nabla \mathbf{q} \cdot \mathbf{n} \, d\ell - \int_{\mathbf{P}} \mathbf{v}_h \cdot \Delta \mathbf{q} \, dA \quad (82)$$

Then, we note that $\Delta \mathbf{q} \in [\mathbb{P}_0(\mathbf{P})]^2$ and the scalar polynomial g satisfying that

$$g = \Delta \mathbf{q} \cdot (\mathbf{x} - \mathbf{x}_{\mathbf{P}}) \quad \text{with} \quad \nabla g = \Delta \mathbf{q} \quad \text{and} \quad \int_{\mathbf{P}} g(\mathbf{x}) \, dA = 0. \quad (83)$$

Using this identity in (82) we see that

$$\begin{aligned}
\int_{\mathbf{P}} \nabla \mathbf{v}_h : \nabla \mathbf{q} \, dA &= \int_{\partial \mathbf{P}} \mathbf{v}_h \cdot \nabla \mathbf{q} \cdot \mathbf{n} \, d\ell - \int_{\mathbf{P}} \mathbf{v}_h \cdot \Delta \mathbf{q} \, dA \\
&= \int_{\partial \mathbf{P}} \mathbf{v}_h \cdot \nabla \mathbf{q} \cdot \mathbf{n} \, d\ell + \int_{\mathbf{P}} (\operatorname{div} \mathbf{v}_h) g \, dA - \int_{\partial \mathbf{P}} g \mathbf{v}_h \cdot \mathbf{n} \, d\ell \\
&= (\mathbf{T1}) + (\mathbf{T2}) + (\mathbf{T3}).
\end{aligned}$$

The boundary integrals **(T1)** and **(T3)** are computable since the trace of \mathbf{v}_h on every edge of $\partial \mathbf{P}$ can be interpolated from its degrees of freedom, while the cell integral **(T2)** is zero because $\operatorname{div} \mathbf{v}_h \in \mathbb{P}_0(\mathbf{P})$ and we have that:

$$(\mathbf{T2}) = \int_{\mathbf{P}} (\operatorname{div} \mathbf{v}_h) g \, dA = (\operatorname{div} \mathbf{v}_h)|_{\mathbf{P}} \int_{\mathbf{P}} g \, dA = 0.$$

Moreover, we can see that $\operatorname{div} \mathbf{v}_h$ is also computable on using the degrees of freedom of \mathbf{v}_h and the divergence theorem:

$$(\operatorname{div} \mathbf{v}_h)|_{\mathbf{P}} |\mathbf{P}| = \int_{\mathbf{P}} \operatorname{div} \mathbf{v}_h \, dA = \int_{\partial \mathbf{P}} \mathbf{v}_h \cdot \mathbf{n} \, d\ell$$

so that

$$(\operatorname{div} \mathbf{v}_h)|_{\mathbf{P}} = \frac{1}{|\mathbf{P}|} \sum_{e \in \partial \mathbf{P}} \int_e \mathbf{v}_h \cdot \mathbf{n} \, d\ell.$$

This formula makes it possible to compute the divergence of \mathbf{v}_h using only the boundary information that can be extracted from **(D1)** and **(D2)**.

To approximate the terms of the MHD variational formulation that depends on the time derivative of the velocity field, we need the L^2 -orthogonal projection of the virtual element vector-valued fields. However, such projection operator is not directly computable in the space $\mathbf{V}_h(\mathbf{P})$, so we change the definition of the space according to the enhancement strategy in [68] that we briefly review below. First, we consider the auxiliary finite dimensional functional spaces

$$\mathcal{G}_2(\mathbf{P}) = \nabla \mathbb{P}_3(\mathbf{P}) \tag{84}$$

and its orthogonal complement in $[\mathbb{P}_2(\mathbf{P})]^2$

$$\mathcal{G}_2^\perp(\mathbf{P}) = \{ \mathbf{g}^\perp \in [\mathbb{P}_2(\mathbf{P})]^2 : (\mathbf{g}^\perp, \mathbf{g})_{\mathbf{P}} = 0 \, \forall \mathbf{g} \in \mathcal{G}_2(\mathbf{P}) \}. \tag{85}$$

Then, we introduce the “extended” virtual element space

$$\begin{aligned}
\mathbf{U}_h(\mathbf{P}) &= \left\{ \mathbf{v}_h \in [H^1(\mathbf{P})]^2 : \mathbf{v}_h|_{\partial \mathbf{P}} \in [\mathbb{B}(\partial \mathbf{P})]^2, \operatorname{div} \mathbf{v}_h \in \mathbb{P}_0(\mathbf{P}) \right. \\
&\quad \left. - \Delta \mathbf{v}_h - \nabla s = \mathbf{g}^\perp \text{ for some } s \in L_0^2(\mathbf{P}), \mathbf{g}^\perp \in \mathcal{G}_2^\perp(\mathbf{P}) \right\}.
\end{aligned} \tag{86}$$

The projector $\Pi_{\mathbf{P}}^\nabla$ can also be defined in $\mathbf{U}_h(\mathbf{P})$ and is computable using only the information from the degrees of freedom **(D1)**-**(D2)**. However, the degrees of freedom **(D1)**-**(D2)** are *not* unisolvent in $\mathbf{U}_h(\mathbf{P})$. Instead, they are unisolvent in $\mathcal{TV}_h(\mathbf{P})$, the subspace of $\mathbf{U}_h(\mathbf{P})$ that is formally defined as

$$\mathcal{TV}_h(\mathbf{P}) = \left\{ \mathbf{v}_h \in \mathbf{U}_h(\mathbf{P}) : \left(\mathbf{v}_h - \Pi_{\mathbf{P}}^\nabla \mathbf{v}_h, \mathbf{g}^\perp \right)_{\mathbf{P}} = 0 \, \forall \mathbf{g}^\perp \in \mathcal{G}_2^\perp(\mathbf{P}) / \mathbb{R}^2 \right\}. \tag{87}$$

Since the degrees of freedom **(D1)**-**(D2)** are unisolvent in this space, we can define the elemental interpolation operator $\mathcal{I}_{\mathbf{P}}^{\mathcal{TV}_h} : [H^1(\mathbf{P})]^2 \rightarrow \mathcal{TV}_h(\mathbf{P})$ such that $\mathbf{u} \in [H^1(\mathbf{P})]^2$ and $\mathcal{I}_{\mathbf{P}}^{\mathcal{TV}_h}(\mathbf{u}) \in \mathcal{TV}_h(\mathbf{P})$ have the same degrees of freedom.

We define the L^2 -orthogonal projection operator $\Pi_{\mathbf{P}}^0 : \mathcal{TV}_h(\mathbf{P}) \rightarrow \mathbf{P}(\mathbf{P})$, so that for every $\mathbf{v}_h \in \mathcal{TV}_h(\mathbf{P})$, the vector polynomial $\Pi_{\mathbf{P}}^0 \mathbf{v}_h$ is the solution to the variational problem

$$(\Pi_{\mathbf{P}}^0 \mathbf{v}_h - \mathbf{v}_h, \mathbf{q})_{\mathbf{P}} = 0. \quad \forall \mathbf{q} \in \mathbf{P}(\mathbf{P}). \tag{88}$$

We show that $\Pi_{\mathbf{P}}^0 \mathbf{v}_h$ is computable using only the degrees of freedom (D1)-(D2) of \mathbf{v}_h . Let $\mathbf{v}_h \in \mathcal{TV}_h(\mathbf{P})$ and $\mathbf{q} \in \mathbf{P}(\mathbf{P})$. We consider the decomposition $\mathbf{q} = \nabla g + \mathbf{g}^\perp$ where $g \in \mathbb{P}_3(\mathbf{P})$ and apply the Green theorem to obtain:

$$\int_{\mathbf{P}} \mathbf{v}_h \cdot \mathbf{q} \, dA = \int_{\mathbf{P}} \mathbf{v}_h \cdot \nabla g \, dA + \int_{\mathbf{P}} \mathbf{v}_h \cdot \mathbf{g}^\perp \, dA. \quad (89)$$

$$= \int_{\partial \mathbf{P}} \mathbf{v}_h \cdot \mathbf{n} g \, d\ell - \int_{\mathbf{P}} \operatorname{div} \mathbf{v}_h g \, dA + \int_{\mathbf{P}} \mathbf{v}_h \cdot \mathbf{g}^\perp \, dA. \quad (90)$$

The boundary integral on the right is computable as the trace of \mathbf{v}_h on every edge is a quadratic polynomial that can be interpolated from the degrees of freedom (D1)-(D2) of \mathbf{v}_h . The second integral in the right-hand side is zero because $\operatorname{div} \mathbf{v}_h|_{\mathbf{P}} \in \mathbb{P}_0(\mathbf{P})$ and we can always take a function g with zero elemental average (alternatively, it can be computed by noting that the divergence of \mathbf{v}_h is given by the divergence theorem). To compute the second integral in (90) we first write

$$\mathbf{g}^\perp = \mathbf{c} + (\mathbf{g}^\perp - \mathbf{c}), \quad \mathbf{c} = \frac{1}{|\mathbf{P}|} \int_{\mathbf{P}} \mathbf{g}^\perp \, dA.$$

Since $\mathbf{c} \in \mathbb{P}_0(\mathbf{P})$ we can find $q \in \mathbb{P}_1(\mathbf{P})$ such that $\mathbf{c} = \nabla q$ and see that

$$\int_{\mathbf{P}} \mathbf{v}_h \cdot \mathbf{c} \, dA = \int_{\partial \mathbf{P}} q \mathbf{v}_h \cdot \mathbf{n} \, d\ell - \int_{\mathbf{P}} \operatorname{div} \mathbf{v}_h q \, dA.$$

Finally, we note that $\mathbf{g}^\perp - \mathbf{c} \in \mathcal{G}_2^\perp(\mathbf{P}) / \mathbb{R}^2$, and the definition of space $\mathcal{TV}_h(\mathbf{P})$ implies that

$$\int_{\mathbf{P}} \mathbf{v}_h \cdot (\mathbf{g}^\perp - \mathbf{c}) \, dA = \int_{\mathbf{P}} \Pi_{\mathbf{P}}^\nabla \mathbf{v}_h \cdot (\mathbf{g}^\perp - \mathbf{c}) \, dA.$$

The last integral is computable because $\Pi_{\mathbf{P}}^\nabla \mathbf{v}_h$ is computable from the degrees of freedom of \mathbf{v}_h and $\mathbf{g}^\perp - \mathbf{c}$ is a known function.

We use the projection operators $\Pi_{\mathbf{P}}^0$ and $\Pi_{\mathbf{P}}^\nabla$ to define the inner product and semi-inner product in $\mathcal{TV}_h(\mathbf{P})$ as follows

$$(\mathbf{u}_h, \mathbf{v}_h)_{\mathcal{TV}_h(\mathbf{P})} = (\Pi_{\mathbf{P}}^0 \mathbf{u}_h, \Pi_{\mathbf{P}}^0 \mathbf{v}_h)_{\mathbf{P}} + \mathcal{S}_{\mathbf{P}}^{\mathcal{TV}_h}((1 - \Pi_{\mathbf{P}}^0) \mathbf{u}_h, (1 - \Pi_{\mathbf{P}}^0) \mathbf{v}_h), \quad (91)$$

$$[\mathbf{u}_h, \mathbf{v}_h]_{\mathcal{TV}_h(\mathbf{P})} = (\nabla \Pi_{\mathbf{P}}^\nabla \mathbf{u}_h, \nabla \Pi_{\mathbf{P}}^\nabla \mathbf{v}_h)_{\mathbf{P}} + \mathcal{T}_{\mathbf{P}}^{\mathcal{TV}_h}(\nabla(1 - \Pi_{\mathbf{P}}^\nabla) \mathbf{u}_h, \nabla(\mathcal{I} - \Pi_{\mathbf{P}}^\nabla) \mathbf{v}_h), \quad (92)$$

for every $\mathbf{u}_h, \mathbf{v}_h$ in $\mathcal{TV}_h(\mathbf{P})$. Here, $\mathcal{S}_{\mathbf{P}}^{\mathcal{TV}_h}$ and $\mathcal{T}_{\mathbf{P}}^{\mathcal{TV}_h}$ are the stabilizing terms, i.e., any continuous bilinear forms for which there exist two pairs of strictly positive constants (t_*, t^*) and (s_*, s^*) , which are independent of h , such that

$$s_* \|\mathbf{v}_h\|_{0,\mathbf{P}}^2 \leq \mathcal{S}_{\mathbf{P}}^{\mathcal{TV}_h}(\mathbf{v}_h, \mathbf{v}_h) \leq s^* \|\mathbf{v}_h\|_{0,\mathbf{P}}^2 \quad \forall \mathbf{v}_h \in \mathcal{TV}_h(\mathbf{P}) \cap \ker(\Pi_{\mathbf{P}}^0), \quad (93)$$

$$t_* \|\nabla \mathbf{v}_h\|_{0,\mathbf{P}}^2 \leq \mathcal{T}_{\mathbf{P}}^{\mathcal{TV}_h}(\nabla \mathbf{v}_h, \nabla \mathbf{v}_h) \leq t^* \|\nabla \mathbf{v}_h\|_{0,\mathbf{P}}^2 \quad \forall \mathbf{v}_h \in \mathcal{TV}_h(\mathbf{P}) \cap \ker(\Pi_{\mathbf{P}}^\nabla). \quad (94)$$

In practice, we can design such stabilizations as in [57, 37]. The inner and semi-inner products respectively defined in (93) and (94) satisfy two fundamental properties, e.g., **Polynomial Consistency** and **Stability**, which are stated in the following theorem.

Theorem 3.14 *The inner product defined in (93) and semi-inner products defined in (94) have the two properties:*

– **Polynomial Consistency:** *for every vector-valued field $\mathbf{v}_h \in \mathcal{TV}_h(\mathbf{P})$ and polynomial $\mathbf{q} \in [\mathbb{P}_2(\mathbf{P})]^2$ it holds that:*

$$(\mathbf{v}_h, \mathbf{q})_{\mathcal{TV}_h(\mathbf{P})} = (\mathbf{v}_h, \mathbf{q})_{\mathbf{P}} \quad \text{and} \quad [\mathbf{v}_h, \mathbf{q}]_{\mathcal{TV}_h(\mathbf{P})} = (\nabla \mathbf{v}_h, \nabla \mathbf{q})_{\mathbf{P}}. \quad (95)$$

– **Stability:** *there exists a pairs of strictly positive constants (t_*, t^*) independent of h such that*

$$t_* \|\mathbf{v}_h\|_{0,\mathbf{P}}^2 \leq (\mathbf{v}_h, \mathbf{v}_h)_{\mathcal{TV}_h(\mathbf{P})} \leq t^* \|\mathbf{v}_h\|_{0,\mathbf{P}}^2, \quad (96)$$

and

$$t_* \|\nabla \mathbf{v}_h\|_{0,\mathbf{P}}^2 \leq [\mathbf{v}_h, \mathbf{v}_h]_{\mathcal{TV}_h(\mathbf{P})} \leq t^* \|\mathbf{v}_h\|_{0,\mathbf{P}}^2. \quad (97)$$

for any $\mathbf{v}_h \in \mathcal{TV}_h(\mathbf{P})$.

Proof. The proof of this theorem uses the same argument of the proof of Theorem 3.3 and is, thus, omitted. \square The

global space \mathcal{TV}_h is given by

$$\mathcal{TV}_h = \{v_h \in [H^1(\Omega)]^2 : \forall P \in \Omega_h \quad v_h|_P \in \mathcal{TV}_h(P)\}.$$

We will endow this space with an inner product and a semi-inner product beginning with their local definitions.

$$(u_h, v_h)_{\mathcal{TV}_h} = \sum_{P \in \Omega_h} (u_h, v_h)_{\mathcal{TV}_h(P)} \quad \forall u_h, v_h \in \mathcal{TV}_h,$$

$$[u_h, v_h]_{\mathcal{TV}_h} = \sum_{P \in \Omega} [u_h, v_h]_{\mathcal{TV}_h(P)} \quad \forall u_h, v_h \in \mathcal{TV}_h.$$

These inner product and semi-inner product induce the norms and semi-norm

$$|||v_h|||_{\mathcal{TV}_h} = (v_h, v_h)_{\mathcal{TV}_h}^{1/2}, \quad |v_h|_{\mathcal{TV}_h} = [v_h, v_h]_{\mathcal{TV}_h}^{1/2}, \quad (98a)$$

$$|||v_h|||_{1, \mathcal{TV}_h} = \left(|||v_h|||_{\mathcal{TV}_h}^2 + |v_h|_{\mathcal{TV}_h}^2 \right)^{1/2}. \quad (98b)$$

The norm in the topological dual space of $\mathcal{TV}_{h,0}$ denoted by $\mathcal{TV}'_{h,0}$ is:

$$|||f_h|||_{-1, \mathcal{TV}_h} = \sup_{v_h \in \mathcal{TV}_{h,0} \setminus \{0\}} \frac{(f_h, v_h)_{\mathcal{TV}_h}}{|v_h|_{\mathcal{TV}_h}}.$$

The global inner product and semi-inner product and their induced norm and semi-norm also satisfy the **consistency** and **stability** properties as stated in the following corollary.

Corollary 3.15 *The norms and semi-norm in (98) are equivalent to the $[L^2(\Omega)]^2$ and $[H^1(\Omega)]^2$ inner products and semi-inner product respectively. In other words, there exists $t_*, t^* > 0$ independent of the mesh characteristics such that for any $v_h \in \mathcal{TV}_h$ it holds that*

$$t_* \|v_h\|_{0,\Omega}^2 \leq |||v_h|||_{\mathcal{TV}_h}^2 \leq t^* \|v_h\|_{0,\Omega}^2, \quad (99a)$$

$$t_* \|\nabla v_h\|_{0,\Omega}^2 \leq |||v_h|||_{\mathcal{TV}_h}^{2,\nabla} \leq t^* \|\nabla v_h\|_{0,\Omega}^2, \quad (99b)$$

$$t_* \|v_h\|_{1,\Omega}^2 \leq |||v_h|||_{1, \mathcal{TV}_h}^2 \leq t^* \|v_h\|_{1,\Omega}^2. \quad (99c)$$

Proof. This result is an immediate consequence of Theorem 3.14 and we omit the proof. \square

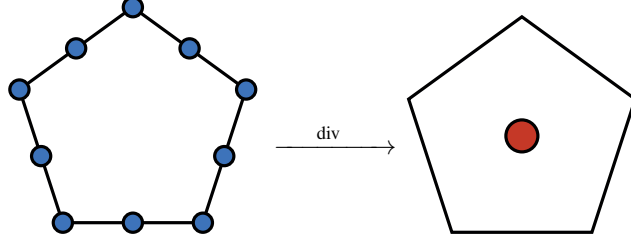
We can define the global interpolation projector $\mathcal{I}^{\mathcal{TV}_h} : [H^1(\Omega)]^2 \rightarrow \mathcal{TV}_h$ that is such that $\mathcal{I}^{\mathcal{TV}_h}(v)|_P = \mathcal{I}_P^{\mathcal{TV}_h}(v|_P)$ for every $P \in \Omega_h$ and $v \in [H^1(\Omega)]^2$. We also define the global space $\mathcal{TV}_{h,0}$ of the functions in \mathcal{TV}_h with zero trace on the boundary of Ω :

$$\mathcal{TV}_{h,0} = \{v_h \in \mathcal{TV}_h : v_h|_{\partial\Omega} \equiv 0\}.$$

We note that the spaces \mathcal{TV}_h and \mathcal{P}_h also form a de Rham complex of the form

$$\begin{array}{ccc} [H^1(\Omega)]^2 & \xrightarrow{\text{div}} & L^2(\Omega) \\ \downarrow \mathcal{I}^{\mathcal{TV}_h} & & \downarrow \mathcal{I}^{\mathcal{P}_h} \\ \mathcal{TV}_h & \xrightarrow{\text{div}} & \mathcal{P}_h \end{array}$$

However, unlike the case presented in subsection 3.5 this chain is not commutative. The set of degrees of freedom are transformed in accordance to the diagram:



Finally, we present a result regarding the stability of the virtual element approximations using the spaces \mathcal{TV}_h and $\mathcal{P}_{h,0}$, which are specifically chosen to satisfy an inf-sup condition.

Theorem 3.16 *There exists a projector $\Pi_h : [H_0^1(\Omega)]^2 \rightarrow \mathcal{TV}_{h,0}$ such that*

$$(\operatorname{div} \Pi_h \mathbf{v}, q_h)_{\mathcal{P}_h} = (\operatorname{div} \mathbf{v}, q_h)_{\mathcal{P}_h} \quad \text{and} \quad \|\Pi_h \mathbf{v}\|_{1, \mathcal{TV}_h} \leq C_\pi \|\mathbf{v}\|_{1, \Omega},$$

for every vector-valued field $\mathbf{v} \in [H_0^1(\Omega)]^2$ and scalar function $q_h \in \mathcal{P}_{h,0}$. Here, C_π is a positive, real constant independent of h . The two spaces \mathcal{TV}_h and $\mathcal{P}_{h,0}$ form an inf-sup stable pair and satisfy

$$\inf_{q_h \in \mathcal{P}_{h,0}} \sup_{\mathbf{v}_h \in \mathcal{TV}_{h,0}} \frac{(\operatorname{div} \mathbf{v}_h, q_h)_{\mathcal{P}_h}}{\|\mathbf{v}_h\|_{1, \mathcal{TV}_h} \|q_h\|_{\mathcal{P}_h}} > \beta_\pi > 0 \quad (100)$$

for some real and strictly positive constant β_π .

This theorem provides a major result since a pair of finite element spaces that do not satisfy such an inf-sup condition will yield unstable simulations of fluid flow phenomena.

4. Energy Estimates

The conforming nature of our VEM allows us to mimic many properties of the continuous setting. Among them, one of the more important is the preservation of certain types of estimates in the $L^2(\Omega)$ -norm, which are obtained by testing the variational formulation against the exact solution and applying Gronwall's lemma, see [43]. In this section, we present an estimate of this type for the continuous system (2a)-(2e) and its discrete counterpart (20a)-(21).

We start with the decompositions

$$\mathbf{u} = \hat{\mathbf{u}} + \mathbf{u}_b \quad \text{and} \quad E = \hat{E} + E_b, \quad (101)$$

where \mathbf{u}_b and E_b are extensions of the boundary conditions inside the domain and $\hat{\mathbf{u}} \in [H_0^1(\Omega)]^2$ and $\hat{E} \in H_0(\mathbf{rot}; \Omega)$ are functions to be found. The extension to the boundary condition of the velocity field is such that

$$\operatorname{div} \mathbf{u}_b = 0 \quad \text{in } \Omega \quad \text{and} \quad \mathbf{u}_b(\mathbf{x}) = \mathbf{0} \quad \text{if } d(\mathbf{x}, \partial\Omega) \geq \epsilon$$

for $h > \epsilon > 0$ for a given threshold ϵ , $d(\mathbf{x}, \partial\Omega)$ being the distance between \mathbf{x} and the boundary $\partial\Omega$. We can construct such an extension \mathbf{u}_b by defining the domain $\Omega_\epsilon = \{\mathbf{x} \in \Omega : d(\mathbf{x}, \partial\Omega) < \epsilon\}$ and taking \mathbf{u}_b to be the solution to the problem:

$$-\Delta \hat{\mathbf{u}}_b + \nabla s = \mathbf{0} \quad \text{in } \Omega_\epsilon, \quad (102a)$$

$$\operatorname{div} \hat{\mathbf{u}}_b = 0 \quad \text{in } \Omega_\epsilon, \quad (102b)$$

$$\hat{\mathbf{u}}_b = \mathbf{u}_b \quad \text{on } \partial\Omega, \quad (102c)$$

$$\hat{\mathbf{u}}_b = \mathbf{0} \quad \text{on } \partial(\Omega \setminus \Omega_\epsilon). \quad (102d)$$

Problem (102) is well-posed, cf. [21]. We further decompose the current density into its values along the boundary and the interior by:

$$\hat{\mathbf{J}} = \hat{E} + \hat{\mathbf{u}} \times \mathbf{B} \quad \text{and} \quad \mathbf{J}_b = E_b + \mathbf{u}_b \times \mathbf{B}.$$

The following theorem gives the continuous energy estimate. Similar estimates are reported in [52, 53, 45].

Theorem 4.1 Let $(\mathbf{u}, \mathbf{B}, E, p)$ solve the variational formulation (15a)-(15d) in the time interval $[0, T]$. Then,

$$\begin{aligned} & \frac{1}{2} \frac{d}{dt} \|\hat{\mathbf{u}}\|_{0,\Omega}^2 + \frac{1}{2R_m} \frac{d}{dt} \|\mathbf{B}\|_{0,\Omega}^2 + R_e^{-1} \|\nabla \hat{\mathbf{u}}\|_{0,\Omega}^2 + \|\hat{J}\|_{0,\Omega}^2 \\ &= (\mathbf{f}, \hat{\mathbf{u}}) - \left(\frac{\partial}{\partial t} \mathbf{u}_b, \hat{\mathbf{u}} \right) - R_e^{-1} (\nabla \mathbf{u}_b, \nabla \hat{\mathbf{u}}) - R_m^{-1} (\mathbf{rot} E_b, \mathbf{B}) - (J_b, \hat{J}), \end{aligned} \quad (103)$$

and

$$\begin{aligned} & \frac{e^{-T}}{2} \|\hat{\mathbf{u}}(T)\|_{0,\Omega}^2 + \frac{e^{-T}}{2R_m} \|\mathbf{B}(T)\|_{0,\Omega}^2 + \int_0^T \left(\frac{e^{-t}}{2R_e} \|\nabla \hat{\mathbf{u}}\|_{0,\Omega}^2 + \frac{e^{-t}}{2} \|\hat{J}\|_{0,\Omega}^2 \right) dt \\ & \leq \frac{e^{-T}}{2} \|\hat{\mathbf{u}}(0)\|_{0,\Omega}^2 + \frac{e^{-T}}{2R_m} \|\mathbf{B}(0)\|_{0,\Omega}^2 \\ & \quad + \int_0^T \left(e^{-t} R_e \|\mathbf{f}\|_{-1,\Omega}^2 + \frac{e^{-t}}{2} \frac{d}{dt} \|\mathbf{u}_b\|_{0,\Omega}^2 + R_e^{-1} e^{-t} \|\nabla \mathbf{u}_b\|_{0,\Omega}^2 \right. \\ & \quad \left. + \frac{e^{-t}}{2R_m} \|\mathbf{rot} E_b\|_{0,\Omega}^2 + \frac{e^{-t}}{2} \|J_b\|_{0,\Omega}^2 \right) dt. \end{aligned} \quad (104)$$

For the discrete version of the estimates presented in Theorem 4.1, for any $n \in [0, N-1]$, we decompose

$$E_h^{n+\theta} = \hat{E}_h^{n+\theta} + \mathcal{I}^{\mathcal{V}_h}(E_b^{n+\theta}), \quad (105)$$

$$\mathbf{u}_h^{n+1} = \hat{\mathbf{u}}_h^{n+1} + \mathcal{I}^{\mathcal{T}\mathcal{V}_h}(\mathbf{u}_b^{n+1}), \quad (106)$$

where $(\hat{E}_h^{n+\theta}, \hat{\mathbf{u}}_h^{n+\theta}) \in \mathcal{V}_{h,0} \times \mathcal{TV}_{h,0}$ and E_b, \mathbf{u}_b are such that their evaluations in $\Omega \setminus \Omega_\epsilon$ are identically zero. The condition on the boundary data is required to guarantee that the degrees of freedom of these boundary fields all lie along the boundary. Next, for any $n, 0 \leq n \leq N-1$, we define

$$\begin{aligned} \hat{J}_h^{n+\theta} &= \hat{E}_h^{n+\theta} + \mathcal{I}^{\mathcal{V}_h}(\hat{\mathbf{u}}_h^{n+\theta} \times \Pi^{RT} \mathbf{B}_h^{n+\theta}), \\ J_{h,b}^{n+\theta} &= \mathcal{I}^{\mathcal{V}_h}(E_b^{n+\theta}) + \mathcal{I}^{\mathcal{V}_h}(\mathbf{u}_b^{n+\theta} \times \Pi^{RT} \mathbf{B}_h^{n+\theta}). \end{aligned}$$

The next result is a discrete counterpart of Theorem 4.1.

Theorem 4.2 Let $\{(u_h^n, \mathbf{B}_h^n)\}_{n=0}^N \subset \mathcal{TV}_h \times \mathcal{E}_h$ and $\{(E_h^{n+\theta}, p_h^{n+\theta})\}_{n=0}^{N-1} \subset \mathcal{V}_h \times \mathcal{P}_{h,0}$ solve the virtual element formulation (20a)-(21). Then, it holds that

$$(\mathbf{L1}) + (\mathbf{L2}) = (\mathbf{R}), \quad (107)$$

where

$$\begin{aligned} (\mathbf{L1}) &= \Delta t (\theta - 1/2) \left(\frac{\|\hat{\mathbf{u}}_h^{n+1} - \hat{\mathbf{u}}_h^n\|_{\mathcal{TV}_h}^2}{\Delta t^2} + \frac{\|\mathbf{B}_h^{n+1} - \mathbf{B}_h^n\|_{\mathcal{E}_h}^2}{\Delta t^2 R_m} \right) \\ & \quad + \left(\frac{\|\hat{\mathbf{u}}_h^{n+1}\|_{\mathcal{TV}_h}^2 - \|\hat{\mathbf{u}}_h^n\|_{\mathcal{TV}_h}^2}{2\Delta t} + \frac{\|\mathbf{B}_h^{n+1}\|_{\mathcal{E}_h}^2 - \|\mathbf{B}_h^n\|_{\mathcal{E}_h}^2}{2\Delta t R_m} \right), \end{aligned} \quad (108a)$$

$$(\mathbf{L2}) = R_e^{-1} \|\hat{\mathbf{u}}_h^{n+\theta}\|_{\mathcal{TV}_h}^2 + \|\hat{J}_h^{n+\theta}\|_{\mathcal{V}_h}^2 + \left(\text{div} \mathcal{I}^{\mathcal{TV}_h} \mathbf{u}_b^{n+\theta}, p_h^{n+\theta} \right)_{\mathcal{P}_h}, \quad (108b)$$

$$\begin{aligned} (\mathbf{R}) &= (\mathbf{f}_h, \hat{\mathbf{u}}_h^{n+\theta})_{\mathcal{TV}_h} - \left(\frac{\mathcal{I}^{\mathcal{TV}_h} \mathbf{u}_b^{n+1} - \mathcal{I}^{\mathcal{TV}_h} \mathbf{u}_b^n}{\Delta t}, \hat{\mathbf{u}}_h^{n+\theta} \right)_{\mathcal{TV}_h} \\ & \quad - R_e^{-1} \left[\mathcal{I}^{\mathcal{TV}_h} \mathbf{u}_b^{n+\theta}, \hat{\mathbf{u}}_h^{n+\theta} \right]_{\mathcal{TV}_h} - (J_{h,b}^{n+\theta}, \hat{J}_h^{n+\theta})_{\mathcal{V}_h} \\ & \quad - R_m^{-1} (\mathbf{rot} \mathcal{I}^{\mathcal{V}_h} E_b^{n+\theta}, \mathbf{B}_h^{n+\theta})_{\mathcal{E}_h}. \end{aligned} \quad (108c)$$

If $\theta \in [1/2, 1]$, for any $\epsilon > 0$ we have that

$$\begin{aligned}
& \alpha^N \left(\|\widehat{\mathbf{u}}_h^N\|_{\mathcal{T}\mathcal{V}_h}^2 + R_m^{-1} \|\mathbf{B}_h^N\|_{\mathcal{E}_h}^2 \right) \\
& + \sum_{n=0}^N \gamma \alpha^n \left(R_e^{-1} |\widehat{\mathbf{u}}_h^{n+\theta}|_{\mathcal{T}\mathcal{V}_h}^2 + \|\widehat{\mathbf{J}}_h^{n+\theta}\|_{\mathcal{V}_h}^2 - 2\epsilon \|\mathbf{p}_h^{n+\theta}\|_{\mathcal{P}_h}^2 \right) \Delta t \\
& \leq \left(\|\mathcal{I}^{\mathcal{T}\mathcal{V}_h}(\mathbf{u}_0)\|_{\mathcal{T}\mathcal{V}_h}^2 + R_m^{-1} \|\mathcal{I}^{\mathcal{E}_h}(\mathbf{B}_0)\|_{\mathcal{E}_h}^2 \right) \\
& + \sum_{n=0}^N \gamma \alpha^n (R_e \|\mathbf{f}_h\|_{-1, \mathcal{T}\mathcal{V}_h}^2 + \Delta t^{-1} \|\mathcal{I}^{\mathcal{T}\mathcal{V}_h}(\mathbf{u}_b^{n+1} - \mathbf{u}_b^n)\|_{\mathcal{T}\mathcal{V}_h}^2 \\
& + R_e^{-1} |\mathcal{I}^{\mathcal{V}_h} \mathbf{u}_b^{n+\theta}|_{\mathcal{T}\mathcal{V}_h}^2 + \frac{\eta^*}{2\epsilon} \left(\int_{\partial\Omega} |\mathcal{I}^{\mathcal{T}\mathcal{V}_h} \mathbf{u}_b^{n+\theta} \cdot \mathbf{n}| ds \right)^2 \\
& + R_m^{-1} \|\mathbf{rot} \mathcal{I}^{\mathcal{V}_h} E_b^{n+\theta}\|_{\mathcal{E}_h}^2 + \|\mathbf{J}_{h,b}^{n+\theta}\|_{\mathcal{V}_h}^2) \Delta t, \tag{109}
\end{aligned}$$

where $\eta^* > 0$ is given in Theorem 3.15 and $\alpha = \theta/(1 + \theta)$ and $\gamma = 1/(1 + \theta)$. Moreover, if $\mathbf{u}_b \cdot \mathbf{n} \equiv 0$ along $\partial\Omega$ (non-penetrating wall condition) we obtain the final energy stability estimate

$$\begin{aligned}
& \alpha^N \left(\|\widehat{\mathbf{u}}_h^N\|_{\mathcal{T}\mathcal{V}_h}^2 + R_m^{-1} \|\mathbf{B}_h^N\|_{\mathcal{E}_h}^2 \right) + \sum_{n=0}^N \gamma \alpha^n \left(R_e^{-1} |\widehat{\mathbf{u}}_h^{n+\theta}|_{\mathcal{T}\mathcal{V}_h}^2 + \|\widehat{\mathbf{J}}_h^{n+\theta}\|_{\mathcal{V}_h}^2 \right) \\
& \leq \left(\|\mathcal{I}^{\mathcal{T}\mathcal{V}_h}(\mathbf{u}_0)\|_{\mathcal{T}\mathcal{V}_h}^2 + R_m^{-1} \|\mathcal{I}^{\mathcal{E}_h}(\mathbf{B}_0)\|_{\mathcal{E}_h}^2 \right) + \sum_{n=0}^N \gamma \alpha^n (R_e \|\mathbf{f}_h\|_{-1, \mathcal{T}\mathcal{V}_h}^2 \\
& + \Delta t^{-1} \|\mathcal{I}^{\mathcal{T}\mathcal{V}_h}(\mathbf{u}_b^{n+1} - \mathbf{u}_b^n)\|_{\mathcal{T}\mathcal{V}_h}^2 + R_e^{-1} |\mathcal{I}^{\mathcal{V}_h} \mathbf{u}_b^{n+\theta}|_{\mathcal{T}\mathcal{V}_h}^2 \\
& + R_m^{-1} \|\mathbf{rot} \mathcal{I}^{\mathcal{V}_h} E_b^{n+\theta}\|_{\mathcal{E}_h}^2 + \|\mathbf{J}_{h,b}^{n+\theta}\|_{\mathcal{V}_h}^2) \Delta t. \tag{110}
\end{aligned}$$

In this section, we are mainly concerned with the development of a solver for the discrete problem (20a)-(21) at a given time instant. For this reason, we keep θ and n fixed, and we omit them from our notation when not strictly necessary. This section is based on the reference [33].

In practice, we manipulate arrays of degrees of freedom of virtual element scalar and vector functions, which we represent as row vectors and denote with the superscript I , e.g., \mathbf{u}_h^I is the row vector of degrees of freedom of \mathbf{u}_h . We introduce the finite dimensional linear space of *column* vectors

$$\mathcal{X}_{h,0} = \left\{ (\mathbf{v}_h^I, \mathbf{C}_h^I, D_h^I, q_h^I)^T : (\mathbf{v}_h, \mathbf{C}_h, D_h, q_h) \in \mathcal{T}\mathcal{V}_{h,0} \times \mathcal{E}_h \times \mathcal{V}_{h,0} \times \mathcal{P}_{h,0} \right\},$$

equipped with the Euclidean (ℓ^2) inner product.

We pose the discrete formulation (20a)-(21) in the space \mathcal{X}_h . In order to exploit symmetry in the Jacobian matrix we replace the discrete form of Faraday's Law (20c) given by

$$\left(\frac{\mathbf{B}_h - \mathbf{B}_h^n}{\Delta t}, \mathbf{C}_h \right)_{\mathcal{E}_h} + (\mathbf{rot} E_h, \mathbf{C}_h)_{\mathcal{E}_h} = 0, \tag{111}$$

with the equivalent expression

$$\theta R_m^{-1} \left(\frac{\mathbf{B}_h - \mathbf{B}_h^n}{\Delta t}, \mathbf{C}_h \right)_{\mathcal{E}_h} + \theta R_m^{-1} (\mathbf{rot} E_h, \mathbf{C}_h)_{\mathcal{E}_h} = 0, \tag{112}$$

and add it to (20a), (20b) and (20d). Then, we define a function $G(\cdot)$ in such a way that $G(\mathbf{x}_h) \cdot \mathbf{y}_h$ is the left hand side of the resulting expression, where we assume that \mathbf{x}_h and \mathbf{y}_h are the column vector given by

$$\mathbf{x}_h = (\widehat{\mathbf{u}}_h^{n+1,I}, \mathbf{B}_h^{n+1,I}, \widehat{E}_h^{n+\theta,I}, p_h^{n+\theta,I})^T \quad \text{and} \quad \mathbf{y}_h = (\mathbf{v}_h^I, \mathbf{C}_h^I, D_h^I, q_h^I)^T.$$

With these positions, the variational formulation (20a)-(21) is equivalent to the problem:

Find $\mathbf{x}_h \in \mathcal{X}_h$ such that

$$G(\mathbf{x}_h) = \mathbf{0}. \tag{113}$$

Indeed, on testing (113) against $\mathbf{y}_h = (\mathbf{v}_h, \mathbf{0}, 0, 0)$ we retrieve (20a), and the other three equations can be attained similarly. This is the set up to apply a Jacobian-free Newton–Krylov method. This method is highly parallelizable and has optimal speed of convergence.

The Newton method at every iteration will produce an updated estimate for the zeroes of G according to

$$\mathbf{x}_h^0 = (\hat{\mathbf{u}}_h^{n,I}, \mathbf{B}_h^{n,I}, \hat{E}_h^{n-1+\theta,I}, p_h^{n-1+\theta,I})^T, \quad (114)$$

$$\mathbf{x}_h^{(m+1)} = \mathbf{x}_h^{(m)} + \delta \mathbf{x}_h^{(m)}, \quad \text{where } \partial G(\mathbf{x}_h^{(m)}) \delta \mathbf{x}_h^{(m)} = -G(\mathbf{x}_h^{(m)}), \quad (115)$$

where $\partial G : \mathcal{X}_{h,0} \rightarrow \mathcal{L}(\mathcal{X}_{h,0})$ is the Jacobian of G , the space $\mathcal{L}(\mathcal{X}_{h,0})$ being the collection of bounded linear operators from $\mathcal{X}_{h,0}$ to its dual space $\mathcal{X}'_{h,0}$. The reason we substitute (20c) with (112) is to attain some symmetry in the Jacobian matrix (which is useful in the well-posedness analysis). The practical implementation of this method requires to compute and store the Jacobian matrix, which may take a lot of computational power and memory. Instead we propose a Jacobian-Free Krylov method.

At each time step we perform a series on Newton iterations where on each iteration we solve a linear system of the form

$$\partial G(\mathbf{x}) \delta \mathbf{x} = -G(\mathbf{x}) \quad (116)$$

We approximate $\delta \mathbf{x}$ using a GMRES iteration. One of the major benefits using GMRES is that we need not know the entries in the Jacobian matrix ∂G . We need only be able to compute the matrix-vector product $\partial G(\mathbf{x}) \delta \mathbf{y}$ for any $\delta \mathbf{y} \in \mathcal{X}_{h,0}$. We can approximate the action of the Jacobian matrix using the operator $DG(\mathbf{x}) : \mathcal{X}_{h,0} \rightarrow \mathcal{X}_{h,0}$ defined using the finite difference approximation:

$$DG(\mathbf{x}_h) \delta \mathbf{x}_h = \frac{G(\mathbf{x}_h + \epsilon \delta \mathbf{x}_h) - G(\mathbf{x}_h)}{\epsilon}, \quad (117)$$

with $\epsilon = 10^{-7}$ (see [48, Page 80]). We emphasize that $DG(\mathbf{x}_h)$ itself is not computed, only its action $DG(\mathbf{x}_h) \delta \mathbf{x}_h$ is. Thus, the algorithm updates $\mathbf{x}_h^{(m+1)}$ from $\mathbf{x}_h^{(m)}$, with $0 \leq m \leq M-1$, as follows:

$$\mathbf{x}_h^{(m+1)} = \mathbf{x}_h^{(m)} + \delta \mathbf{x}_h^{(m)}, \quad \text{where } DG(\mathbf{x}_h^{(m)}) \delta \mathbf{x}_h^{(m)} = -G(\mathbf{x}_h^{(m)}), \quad (118a)$$

$$\text{with the initial guess } \mathbf{x}_h^{(0)} = \begin{cases} (\hat{\mathbf{u}}_h^{n,I}, \mathbf{B}_h^{n,I}, \hat{E}_h^{n-1+\theta,I}, p_h^{n-1+\theta,I})^T & n > 0, \\ (\hat{\mathbf{u}}_h^{0,I}, \mathbf{B}_h^{0,I}, 0, 0)^T & n = 0. \end{cases} \quad (118b)$$

We define intermediate approximations at iteration m and the final values through the degrees of freedom of $\mathbf{x}_h^{(m)}$ and $\mathbf{x}_h^{(M)}$, respectively:

$$\begin{aligned} (\hat{\mathbf{u}}_h^{n+1,(m),I}, \mathbf{B}_h^{n+1,(m),I}, \hat{E}_h^{n+\theta,(m),I}, p_h^{n+\theta,(m),I})^T &= \mathbf{x}_h^{(m)}, \\ (\hat{\mathbf{u}}_h^{n+1}, \mathbf{B}_h^{n+1}, \hat{E}_h^{n+\theta}, p_h^{n+\theta}) &= \mathbf{x}_h^{(M)}. \end{aligned}$$

This Krylov method requires a user-defined input tolerance η_m that we fix as follows:

$$\|DG(\mathbf{x}_h^{(m)}) \delta \mathbf{x}_h^{(m)} + G(\mathbf{x}_h^{(m)})\|_2 \leq \eta_m \|G(\mathbf{x}_h^{(m)})\|_2, \quad (119a)$$

$$\eta_m = \min \left\{ \eta_{\max}, \max \left(\eta_m^B, \gamma \frac{\epsilon_t}{\|G(\mathbf{x}_h^{(m)})\|_2} \right) \right\}, \quad (119b)$$

$$\eta_m^B = \min \{ \eta_{\max}, \max (\eta_m^A, \gamma \eta_{m-1}^\alpha) \}, \quad \eta_m^A = \gamma \left(\frac{\|G(\mathbf{x}_h^{(m)})\|_2}{\|G(\mathbf{x}_h^{(m-1)})\|_2} \right)^\alpha. \quad (119c)$$

with $\alpha = 1.5, \gamma = 0.9, \eta_{\max} = 0.8$. The value of ϵ_t is chosen to guarantee that the non-linear convergence has been achieved.

$$\|G(\mathbf{x}_h^{(m)})\|_2 < \epsilon_a + \epsilon_r \|G(\mathbf{x}_h^{(0)})\|_2 = \epsilon_t, \quad (120)$$

$$\epsilon_a = \sqrt{\#\text{dof}} \times 10^{-15}, \quad \epsilon_r = 10^{-4}. \quad (121)$$

Where $\#\text{dof}$ is the sum of the number of degrees of freedom in each of our modeling spaces. The value of these parameters is chosen in accordance with [7]. However, this strategy is much more general [42]. The guiding philosophy being a desire to guarantee super-linear convergence while simultaneously not over-solving with unnecessary GMRES iterations.

The non-linear nature of the inexact Newton steps may shed doubt as to whether or not this solver preserves the divergence free nature of the magnetic field. The following result is a consequence of the Faraday law. Note that the finite difference approximation to its Jacobian is exact since the Faraday law is linear.

Theorem 4.3 *Suppose $\delta\mathbf{x}_h$ is a solution of the linear problem*

$$DG(\mathbf{x}_h)\delta\mathbf{x}_h = -G(\mathbf{x}_h). \quad (122)$$

Then we have the following relation for the $\delta\mathbf{B}_h$ component of $\delta\mathbf{x}_h$

$$\text{div } \delta\mathbf{B}_h = \text{div } (\mathbf{B}_h^n - \mathbf{B}_h). \quad (123)$$

Proof 4 *Testing (122) against $\mathbf{y}_h = (0, \mathbf{C}_h^I, 0, 0)$ yields*

$$\Delta t^{-1} \left(\delta\mathbf{B}_h, \mathbf{C}_h \right)_{\varepsilon_h} + \left(\text{rot } \delta\hat{\mathbf{E}}_h, \mathbf{C}_h \right)_{\varepsilon_h} - \left(\frac{\mathbf{B}_h - \mathbf{B}_h^n}{\Delta t}, \mathbf{C}_h \right)_{\varepsilon_h} - \left(\text{rot } \hat{\mathbf{E}}_h, \mathbf{C}_h \right)_{\varepsilon_h} = 0.$$

Since \mathbf{C}_h can be selected arbitrarily, the relation above is equivalent to

$$\Delta t^{-1} [\delta\mathbf{B}_h + \mathbf{B}_h - \mathbf{B}_h^n] = -\text{rot } (\delta\hat{\mathbf{E}}_h + \hat{\mathbf{E}}_h). \quad (124)$$

The assertion of the theorem follows by taking the divergence of both sides.

Corollary 4.4 *If the initial conditions on the magnetic field \mathbf{B}_0 satisfy that $\text{div } \mathbf{B}_0 = 0$ then updates defined by (118) will satisfy that*

$$\text{div } \delta\mathbf{B}_h^{n,(m)} = 0 \quad \forall n \in [0, N], m \in [0, M].$$

implying that

$$\text{div } \mathbf{B}_h^n = 0 \quad \forall n \in [0, N].$$

Proof 5 *The divergence of the initial estimate can be computed using the commuting property of the diagram in Theorem 3.12. Indeed,*

$$\text{div } \mathbf{B}_h^0 = \text{div } \mathcal{I}^{\varepsilon_h}(\mathbf{B}_0) = \mathcal{I}^{\mathcal{P}_h}(\text{div } \mathbf{B}_0) = 0.$$

Next, suppose that $\text{div } {}_h\mathbf{B}_h^n = 0$. Then, by definition we have that $\text{div } \mathbf{B}_h^{n+1,0} = 0$. For the inductive step we can further assume that $\text{div } \mathbf{B}_h^{n+1,m} = 0$, so that from Theorem 4.3 we find that

$$\text{div } \mathbf{B}_h^{n+1,(m+1)} = \text{div } \mathbf{B}_h^{n+1,(m)} + \text{div } \delta\mathbf{B}_h^{n+1,(m)} = \text{div } (2\mathbf{B}_h^{n+1,(m)} - \mathbf{B}_h^n) = 0,$$

which implies that assertion of the corollary.

5. Well-posedness and stability of the linear solver

The linearization strategy laid out in subsection 4 can be summarized as follows. We are given a set of initial conditions. Then, at each time step we perform a series of Newton iterations, each one of these requiring the solution $\delta\mathbf{x}_h \in \mathcal{X}_{h,0}$ of a linear system like:

$$\partial G(\mathbf{x}_h)\delta\mathbf{x}_h = -G(\mathbf{x}_h). \quad (125)$$

for any given $\mathbf{x}_h \in \mathcal{X}_{h,0}$. To compute the Jacobian $\partial G(\mathbf{x}_h)$ we use the definition:

$$[\partial G(\mathbf{x}_h)\delta\mathbf{x}_h] \cdot \mathbf{y}_h = \lim_{\epsilon \rightarrow 0} \frac{G(\mathbf{x}_h + \epsilon\delta\mathbf{x}_h) \cdot \mathbf{y}_h - G(\mathbf{x}_h) \cdot \mathbf{y}_h}{\epsilon}. \quad (126)$$

The limit above yields

$$[\partial G(\mathbf{x}_h)\delta\mathbf{x}_h] \cdot \mathbf{y}_h = \ell_1(\mathbf{y}_h) + \ell_2(\mathbf{y}_h) + \ell_3(\mathbf{y}_h) + \ell_4(\mathbf{y}_h), \quad (127)$$

where $\mathbf{x}_h = (\hat{\mathbf{u}}_h^I, \mathbf{B}_h^I, \hat{E}_h^I, p_h^I)^T$, $\delta \mathbf{x}_h = (\delta \hat{\mathbf{u}}_h^I, \delta \mathbf{B}_h^I, \delta \hat{E}_h^I, \delta p_h^I)^T$,
 $\mathbf{y}_h = (\mathbf{v}_h^I, \mathbf{C}_h^I, D_h^I, q_h^I)^T$, and

$$\begin{aligned}\ell_1(\mathbf{y}_h) &= \Delta t^{-1} \left(\delta \hat{\mathbf{u}}_h, \mathbf{v}_h \right)_{\mathcal{TV}_h} + \theta R_e^{-1} \left[\delta \hat{\mathbf{u}}_h, \mathbf{v}_h \right]_{\mathcal{TV}_h} \\ &\quad + \theta \left(\hat{E}_h, \mathcal{I}^{\mathcal{V}_h}(\mathbf{v}_h \times \Pi^{RT} \delta \mathbf{B}_h) \right)_{\mathcal{V}_h} \\ &\quad + \theta \left(\delta \hat{E}_h, \mathcal{I}^{\mathcal{V}_h}(\mathbf{v}_h \times \Pi^{RT} \mathbf{B}_h) \right)_{\mathcal{V}_h} - \left(\operatorname{div} \mathbf{v}_h, p_h \right)_{\mathcal{P}_h}, \\ \ell_2(\mathbf{y}_h) &= \theta \left(\operatorname{div} \delta \hat{\mathbf{u}}_h, q_h \right)_{\mathcal{P}_h}, \\ \ell_3(\mathbf{y}_h) &= \Delta t^{-1} \left(\delta \mathbf{B}_h, \mathbf{C}_h \right)_{\mathcal{E}_h} + \left(\operatorname{rot} \delta E_h, \mathbf{C}_h \right)_{\mathcal{E}_h}, \\ \ell_4(\mathbf{y}_h) &= \left(\delta \hat{E}_h + \theta \mathcal{I}^{\mathcal{V}_h}(\hat{\mathbf{u}}_h \times \Pi^{RT} \delta \mathbf{B}_h + \delta \hat{\mathbf{u}}_h \times \Pi^{RT} \mathbf{B}_h), D_h \right)_{\mathcal{V}_h} \\ &\quad + R_m^{-1} \theta \left(\delta \mathbf{B}_h, \operatorname{rot}_h D_h \right)_{\mathcal{E}_h}.\end{aligned}$$

These linear systems are in the form of a saddle-point problem satisfying the hypothesis of the following theorem, which can be used to prove the well posedness.

Theorem 5.1 *Let U and P be Hilbert spaces respectively endowed with the norms $\|\cdot\|_U$ and $\|\cdot\|_P$. Let $a : U \times U \rightarrow \mathbb{R}$, $b : U \times P \rightarrow \mathbb{R}$ be two bounded bilinear forms satisfying the inf-sup conditions*

$$\inf_{u \in U_0} \sup_{v \in U_0} \frac{a(u, v)}{\|u\|_U \|v\|_U} > 0, \quad \inf_{p \in P} \sup_{u \in U} \frac{b(u, p)}{\|u\|_U \|p\|_P} > 0, \quad (128)$$

where

$$U_0 = \{u \in U : \forall p \in P \quad b(u, p) = 0\}. \quad (129)$$

Then, for every pair of bounded linear functionals $f \in U'$ and $g \in P'$ there exists unique $u \in U$ and $p \in P$ such that for any $v \in U$ and $q \in P$ it is the case that

$$\begin{aligned}a(u, v) - b(v, p) &= f(v) & \forall v \in U, \\ b(u, q) &= g(q) & \forall q \in P.\end{aligned}$$

Moreover there exists a constant $C > 0$ independent of f and g such that

$$\|u\|_U + \|p\|_P \leq C (\|f\|_{U'} + \|g\|_{P'}), \quad (130)$$

with the (standard) definition of the norms in the dual spaces:

$$\|f\|_{U'} = \sup_{u \in U \setminus \{0\}} \frac{|f(u)|}{\|u\|_U}, \quad \|g\|_{P'} = \sup_{p \in P \setminus \{0\}} \frac{|g(p)|}{\|p\|_P}. \quad (131)$$

Proof. A proof of this theorem can be found in [26, 21]. \square

Consider the space:

$$\mathfrak{X}_h = \mathcal{TV}_{h,0} \times \mathcal{E}_h \times \mathcal{V}_{h,0}, \quad (132)$$

and the bilinear form $a_h : \mathfrak{X}_h \times \mathfrak{X}_h \rightarrow \mathbb{R}$, whose evaluation at $\delta \boldsymbol{\xi}_h = (\delta \hat{\mathbf{u}}_h, \delta \mathbf{B}_h, \delta \hat{E}_h)$, $\boldsymbol{\eta}_h = (\mathbf{v}_h, \mathbf{C}_h, D_h)$ is given by $a_h(\delta \boldsymbol{\xi}_h, \boldsymbol{\eta}_h) = \ell_1(\mathbf{v}_h) + \ell_2(\mathbf{C}_h) + \ell_3(D_h)$, cf. equation (127). Here, and for the remainder of the section, we fix the value $\mathbf{x}_h = (\hat{\mathbf{u}}_h, \mathbf{B}_h, \hat{E}_h)$. We can reformulate problem (125) as:

Find $(\delta \boldsymbol{\xi}_h, \delta p_h) \in \mathfrak{X}_h \times \mathcal{P}_{h,0}$ such that for all $(\boldsymbol{\eta}_h, q_h) \in \mathfrak{X}_h \times \mathcal{P}_{h,0}$ it holds that

$$a_h(\delta \boldsymbol{\xi}_h, \boldsymbol{\eta}_h) - b_h(\mathbf{v}_h, \delta p_h) = f(\boldsymbol{\eta}_h), \quad (133a)$$

$$b_h(\delta \hat{\mathbf{u}}_h, q_h) = g(q_h), \quad (133b)$$

Where $f \in \mathfrak{X}'_h$ and $g \in \mathcal{P}'_{h,0}$ are some appropriate bounded linear functionals and

$$b_h(\mathbf{v}_h, q_h) = (\operatorname{div} \mathbf{v}_h, q_h)_{\mathcal{P}_h}. \quad (134)$$

The strategy we follow to prove the well-posedness of the virtual element approximation proceeds in three steps:

- (i) we introduce an auxiliary problem;
- (ii) we show that the auxiliary problem and problem (133) are equivalent;
- (iii) we show that the auxiliary problem is well posed.

In the rest of this section we briefly sketch the various steps of this argument, see Chapter 5 in [63] for details.

The auxiliary problem is given by: Find $(\delta\xi_h, \delta p_h) \in \mathfrak{X}_h \times \mathcal{P}_{h,0}$ such that for all $(\eta_h, q_h) \in \mathfrak{X}_h \times \mathcal{P}_{h,0}$ it holds that

$$a_{h,0}(\delta\xi_h, \eta_h) - b_h(\mathbf{v}_h, \delta p_h) = f_h(\eta_h), \quad (135a)$$

$$b_h(\delta\hat{\mathbf{u}}_h, q_h) = g_h(q_h). \quad (135b)$$

Note that

$$a_{h,0}(\delta\xi_h, \eta_h) = a_h(\delta\xi_h, \eta_h) + \theta R_m^{-1} \left(\operatorname{div} \delta \mathbf{B}_h, \operatorname{div} \mathbf{C}_h \right)_{\mathcal{P}_h}. \quad (136)$$

Then, to establish the equivalence between (133) and (135), we need to ensure that approximations using the auxiliary problem (135) will have divergence free magnetic fields. This is settled in the following Theorem:

Theorem 5.2 *Let $\delta\xi_h = (\delta\hat{\mathbf{u}}_h, \delta\mathbf{B}_h, \delta\hat{E}_h) \in \mathfrak{X}_h$ and $p_h \in \mathcal{P}_{h,0}$ solve (135). If the initial conditions on the magnetic field are divergence free, then it holds that $\operatorname{div} \delta\mathbf{B}_h = 0$.*

We can leverage the result of this theorem to show that both problems (133) and (135) are equivalent as stated by the following lemma.

Lemma 5.3 *The problems (133) and (135) are equivalent.*

Finally, we present the well-posedness of (135). Following the framework laid out in [45], we introduce the norm on $\mathfrak{X}_{h,0}$ such that for any $\xi_h = (\mathbf{u}_h, \mathbf{B}_h, E_h) \in \mathfrak{X}_{h,0}$ we have

$$\|\xi_h\|_{\mathfrak{X}_{h,0}}^2 := \|\mathbf{v}_h\|_{\Delta t, \nabla}^2 + \|E_h\|_{\Delta t, \operatorname{rot}}^2 + \|\mathbf{B}_h\|_{\Delta t, \operatorname{div}}^2, \quad (137a)$$

$$\|\mathbf{u}_h\|_{\Delta t, \nabla}^2 := \Delta t^{-1} \|\mathbf{u}_h\|_{\mathcal{T}\mathcal{V}_h}^2 + |\mathbf{u}_h|_{\mathcal{T}\mathcal{V}_h}^2 + \Delta t^{-1} \|\operatorname{div} \mathbf{u}_h\|_{\mathcal{P}_h}^2, \quad (137b)$$

$$\|\mathbf{B}_h\|_{\Delta t, \operatorname{div}}^2 := \Delta t^{-1} \|\mathbf{B}_h\|_{\varepsilon_h}^2 + \|\operatorname{div} \mathbf{B}_h\|_{\mathcal{P}_h}^2, \quad (137c)$$

$$\|E_h\|_{\Delta t, \operatorname{rot}}^2 := \|E_h\|_{\mathcal{V}_h}^2 + \Delta t \|\operatorname{rot} E_h\|_{\varepsilon_h}^2. \quad (137d)$$

Well-posedness relies on Theorem 5.1. The first hypothesis established that the bilinear forms in the formulation of (135) are continuous

Lemma 5.4 *Suppose that $\Delta t^{1/2} \hat{\mathbf{u}}_h, \hat{\mathbf{u}}_h, \mathbf{B}_h \in [L^\infty(\Omega)]^2$ and $\hat{E}_h \in L^\infty(\Omega)$. Then, the bilinear form $a_{h,0}$ is continuous in the norms defined in (137a).*

The next lemma guarantees that the bilinear form $a_{h,0}$ satisfies the inf-sup condition.

Lemma 5.5 *Let $\theta > 0$, and $\hat{\mathbf{u}}_h, \mathbf{B}_h \in [L^\infty(\Omega)]^2$ and $\hat{E}_h \in L^\infty(\Omega)$. For a Δt small enough, we have that*

$$\inf_{\delta\xi_h \in \mathfrak{X}_{h,0}} \sup_{\eta_h \in \mathfrak{X}_{h,0}} \frac{a_{h,0}(\delta\xi_h, \eta_h)}{\|\delta\xi_h\|_{\mathfrak{X}_{h,0}} \|\eta_h\|_{\mathfrak{X}_{h,0}}} \geq C > 0,$$

where $\mathfrak{X}_{h,0} = \{(\mathbf{v}_h, \mathbf{B}_h, E_h) : \operatorname{div} \mathbf{v}_h = 0\}$ and C is a strictly positive, real constant independent of h and Δt .

6. Numerical Experiments

In this section, we show some numerical results for the approximation of the subsystem of (2a)-(2e) that describes the electromagnetic part of the MHD model.

$$\frac{\partial}{\partial t} \mathbf{B} + \operatorname{rot} E = \mathbf{0} \quad \text{in } \Omega, \quad (138a)$$

$$E + \mathbf{u} \times \mathbf{B} - R_m^{-1} \operatorname{rot} \mathbf{B} = \mathbf{0} \quad \text{in } \Omega, \quad (138b)$$

$$\mathbf{B}(0) = \mathbf{B}_0 \quad \text{in } \Omega \quad (138c)$$

$$E \equiv E_b \quad \text{along } \partial\Omega. \quad (138d)$$

We present an experimental study of the convergence properties of the VEM and show the performance when we apply the VEM to the numerical modeling of a magnetic reconnection model.

6.1. Experimental Study of Convergence

The first test that we perform regards the convergence rate of the VEM. We consider the computational domain $\Omega = [-1, 1] \times [-1, 1]$ partitioned by three different mesh families, a triangular mesh, a perturbed quadrilateral mesh and a Voronoi Tessellation. We assume that an external velocity field $\mathbf{u} = (u_x, u_y)^T$ is imposed, whose components are

$$u_x(x, y) = -\frac{(x^2 + y^2 - 1)(\sin(xy) + \cos(xy)) - 100e^x + 100e^y}{2(50e^x - y \sin(xy) + y \cos(xy))}, \quad (139)$$

$$u_y(x, y) = \frac{(x^2 + y^2 - 1)(\sin(xy) + \cos(xy)) - 100e^x + 100e^y}{2(50e^y + x \sin(xy) - x \cos(xy))}. \quad (140)$$

The initial and the boundary conditions are set in accordance with the electric and magnetic fields, which we assume as the exact solutions.

$$\mathbf{B}(x, y, t) = \begin{pmatrix} 50e^y + x \sin(xy) - x \cos(xy) \\ 50e^x - y \sin(xy) + y \cos(xy) \end{pmatrix} e^{-t}, \quad (141)$$

$$E(x, y, t) = -(50(e^x - e^y) + \cos(xy) + \sin(xy))e^{-t}. \quad (142)$$

The simulation uses the time discretization given by $\theta = 1/2$ and time step $\Delta t = 0.05h^2$, and we integrate from $t = 0$ to $t = T$, the final time being $T = 0.25$. We measure the relative errors of E and \mathbf{B} through the mesh dependent norms of the difference between the exact and numerical solutions divided by the norm of the exact solution. The results are shown in Figure 5. In each plot, we show three different convergence curves. These curves refer to the three different possibilities that we presented in subsubsection 3.2.1 for the construction of the inner product in the space \mathcal{V}_h . These plots provide evidence that the convergence rate for the electric field is quadratic while the convergence rate for the magnetic field is linear. In the case of Voronoi tessellations the convergence plots associated with the inner product defined by the Galerkin interpolator (GI) show some irregular behavior. These types of meshes may have arbitrarily small edges conflicting with the criteria normally used in the VEM. Another possible explanation may have to do with the G.I, note that this irregular behavior does not happen with the other two sample inner products.

An important feature of the VEM is that the divergence of the magnetic field should remain zero throughout the simulation. In Figure 6 we show plots of the evolution of the L^2 -norm of the divergence of the magnetic field. These show that this quantity remains very close, in norm, to the machine epsilon.

6.2. Magnetic Reconnection

The next numerical experiment involves a characteristic feature of resistive MHD – the phenomenon of magnetic reconnection. At very large scales, usually in space physics, the behavior of plasmas can be well-approximated using ideal MHD. In this case, according to the Alfvén’s Theorem, the magnetic field lines will advect with the fluid, see Section 4.3 in [38] for a full discussion. This feature is often referred to as the “frozen-in” condition on the magnetic field. In certain regions of the Earth’s magnetosphere, namely the magnetopause and magnetotail, the magnetic reconnection will lead to very thin current sheets that separate regions across which the magnetic field changes substantially.

In this numerical experiment, we consider one Harris sheet constrained to the computational domain $\Omega = [-1, 1]^2$ and given by the following profile of the magnetic field, first introduced in [44],

$$\mathbf{B}_0(x, y) = (\tanh y, 0). \quad (143)$$

The simplicity of this condition has made it a popular choice in modeling magnetic reconnection. We will use the expression (143) as the initial condition for the magnetic field. We will further assume that the particles in this sheet are subjected by some external agent to a flow described by

$$\mathbf{u}(x, y, t) = (-x, y). \quad (144)$$

This flow will force the magnetic field lines to come together at a single point making the current density grow. The system becomes highly unstable and the magnetic field lines begin to tear apart, this phenomenon is called a tearing

instability and magnetic reconnection happens as a response. This process is described in detail in [49, 66]. We close this model by imposing the boundary conditions

$$\forall t > 0 : \quad E_b(t) \in \mathbb{P}_0(\partial\Omega), \quad \text{and} \quad \int_{\partial\Omega} \mathbf{B}_b(t) \cdot \mathbf{n} d\ell = 0 \quad (145)$$

The mesh we are using is refined near the center of the domain Ω , to guarantee higher resolution in the region of space where the phenomenon of magnetic reconnection occurs. The downside of using such a mesh is that a series of hanging nodes are introduced. This numerical experiment demonstrates the versatility of the VEM, and the advantage of this method over more classical methods like the FEM or FDM.

In Fig. 7 we display the mesh used along with a set of frames displaying the evolution in time of the magnetic field. The phenomenon of magnetic reconnection begins at $T = 0$ and by $T = 0.450$ a steady state is achieved.

7. Conclusions

In this chapter, we developed a VEM for the PDE system of resistive MHD. In developing this chapter we have introduced two chains of spaces, see subsections 3.5 and the final results in 3.6. One chain of spaces is aimed at approximating the electromagnetics submodel, while the other applies to the submodel for fluid flow. There are terms in the MHD equations that couple the two submodels that require information about both the phenomena of electromagnetics and fluid flow. Special care needs to be taken in discretizing these terms so that the fully discretized MHD system satisfies discrete (stability) energy estimates. These estimates are the main result of section 4. They guarantee the stability of the method.

The VEM, when applied to MHD, yields a large system of non-linear equations. In order to arrive at approximate solutions a linearization strategy has to be developed. In section 4 we developed a Newton iteration to address this issue. We were able to prove that this linearization strategy will preserve the divergence of the magnetic field such that if the initial conditions are divergence free then these non-linear iterations will preserve this divergence free property in the discrete mesh. The analysis of section 5 shows that the set of linear systems that need to be solved are, in fact, well-posed saddle point problems. This well-posedness result serves as a first step into developing robust preconditioners following the framework presented in [54].

In section 6 we also presented a series of numerical experiments exploring the subsystem that describes the electromagnetics. These experiments show that the (lowest-order) VEM is convergent, the speed of convergence is quadratic for the electric field and linear for the magnetic field. Further experimentation shows that the divergence of the magnetic field remains well below machine epsilon. We also present a model for a phenomenon characteristic of resistive MHD, that of magnetic reconnection. This model accurately describes the behavior of plasmas in tokamaks as well as many electromagnetic interactions in the magnetosphere of a planet. Our compatible discretization closely mimics the behavior of the exact solution to our model. This model was discretized on a mesh that was refined near the center of the computational domain where reconnection will happen. Using this mesh will provide higher resolution in the parts of the domain where such resolution is required and aids in saving computational resources. Other numerical methods struggle with this type of mesh because it introduces a series of hanging nodes. However, the VEM performs just as well in this type of mesh.

Acknowledgement

Dr. S. Naranjo Alvarez's work was supported by the National Science Foundation (NSF) grant #1545188, "*NRT-DESE: Risk and uncertainty quantification in marine science and policy*", which provided a one year fellowship and internship support at Los Alamos National Laboratory. Dr. S. Naranjo Alvarez also received graduate research funding from Professor V. A. Bokil's DMS grant #1720116 and # 2012882, an INTERN supplemental award to Professor Bokil's DMS grant # 1720116 for a second internship at Los Alamos National Laboratory, and teaching support from the Department of Mathematics at Oregon State University. In addition, S. Naranjo Alvarez was also supported by the DOE-ASCR AM (Applied Math) base program grant for a summer internship.

Professor V. A. Bokil was partially supported by NSF funding from the DMS grants # 1720116 and # 2012882.

Dr. V. Gyrya and Dr. G. Manzini were supported by the LDRD-ER program of Los Alamos National Laboratory under project number 20180428ER.

The authors would like to thank Dr. K. Lipnikov and Dr. L. Chacon, T-5 Group, Theoretical Division, Los Alamos National Laboratory, for their advice during the writing of this article.

Los Alamos National Laboratory is operated by Triad National Security, LLC, for the National Nuclear Security Administration of U.S. Department of Energy (Contract No. 89233218CNA000001).

References

- [1] B. Ahmad, A. Alsaedi, F. Brezzi, L. D. Marini, and A. Russo. Equivalent projectors for virtual element methods. *Computers & Mathematics with Applications*, 66(3):376–391, 2013.
- [2] P. F. Antonietti, L. Beirão da Veiga, S. Scacchi, and M. Verani. A C^1 virtual element method for the Cahn-Hilliard equation with polygonal meshes. *SIAM J. Numer. Anal.*, 54(1):34–56, 2016.
- [3] P. F. Antonietti, G. Manzini, and M. Verani. The conforming virtual element method for polyharmonic problems. *Comput. Math. Appl.*, 79(7):2021–2034, 2020.
- [4] L. Beirão da Veiga, F. Brezzi, A. Cangiani, G. Manzini, L. D. Marini, and A. Russo. Basic principles of virtual element methods. *Mathematical Models & Methods in Applied Sciences*, 23(01):199–214, 2013.
- [5] L. Beirão da Veiga, F. Brezzi, F. Dassi, L. D. Marini, and A. Russo. Virtual element approximation of 2D magnetostatic problems. *Computer Methods in Applied Mechanics and Engineering*, 327:173–195, 2017.
- [6] L. Beirão da Veiga, F. Brezzi, F. Dassi, L. D. Marini, and A. Russo. Lowest order virtual element approximation of magnetostatic problems. *Computer Methods in Applied Mechanics and Engineering*, 332:343–362, 2018.
- [7] L. Beirão da Veiga, F. Brezzi, D. Marini, and A. Russo. Mixed virtual element methods for general second order elliptic problems on polygonal meshes. *ESAIM: Mathematical Modelling and Numerical Analysis*, 50(3):727–747, 2016.
- [8] L. Beirão da Veiga, F. Brezzi, L. D. Marini, and A. Russo. The hitchhiker’s guide to the virtual element method. *Mathematical Models & Methods in Applied Sciences*, 24(08):1541–1573, 2014.
- [9] L. Beirão da Veiga, F. Brezzi, L. D. Marini, and A. Russo. H(div) and H(curl)-conforming VEM. *Numer. Math.*, 133(2):303–332, 2016.
- [10] L. Beirão da Veiga, F. Brezzi, L. D. Marini, and A. Russo. Virtual element methods for general second order elliptic problems on polygonal meshes. *Math. Models Methods Appl. Sci.*, 26(4):729–750, 2016.
- [11] L. Beirão da Veiga, A. Chernov, L. Mascotto, and A. Russo. Basic principles of hp virtual elements on quasiuniform meshes. *Math. Models Methods Appl. Sci.*, 26(8):1567–1598, 2016.
- [12] L. Beirão da Veiga, K. Lipnikov, and G. Manzini. Arbitrary order nodal mimetic discretizations of elliptic problems on polygonal meshes. *SIAM Journal on Numerical Analysis*, 49(5):1737–1760, 2011.
- [13] L. Beirão da Veiga, K. Lipnikov, and G. Manzini. *The Mimetic Finite Difference Method*, volume 11 of *MS&A. Modeling, Simulations and Applications*. Springer, 1 edition, 2014.
- [14] L. Beirão da Veiga, C. Lovadina, and A. Russo. Stability analysis for the virtual element method. *Mathematical Models and Methods in Applied Sciences*, 27(13):2557–2594, 2017.
- [15] L. Beirão da Veiga, C. Lovadina, and G. Vacca. Divergence free virtual elements for the Stokes problem on polygonal meshes. *ESAIM: Mathematical Modelling and Numerical Analysis*, 51(2):509–535, 2017.
- [16] L. Beirão da Veiga, C. Lovadina, and G. Vacca. Virtual elements for the Navier–Stokes problem on polygonal meshes. *SIAM Journal on Numerical Analysis*, 56(3):1210–1242, 2018.
- [17] L. Beirão da Veiga and G. Manzini. Residual *a posteriori* error estimation for the virtual element method for elliptic problems. *ESAIM Math. Model. Numer. Anal.*, 49(2):577–599, 2015.
- [18] L. Beirão da Veiga, F. Brezzi, F. Dassi, L. D. Marini, and A. Russo. A family of three-dimensional virtual elements with applications to magnetostatics. *SIAM J. Numer. Anal.*, 56(5):2940–2962, 2018.
- [19] E. Benvenuti, A. Chiozzi, G. Manzini, and N. Sukumar. Extended virtual element method for the Laplace problem with singularities and discontinuities. *Comput. Methods Appl. Mech. Engrg.*, 356:571 – 597, 2019.
- [20] S. Berrone, S. Pieraccini, S. Scialò, and F. Vicini. A parallel solver for large scale DFN flow simulations. *SIAM J. Sci. Comput.*, 37(3):C285–C306, 2015.
- [21] D. Boffi, F. Brezzi, and M. Fortin. *Mixed finite element methods and applications*, volume 44. Springer, 2013.
- [22] J. Brackbill. Fluid modeling of magnetized plasmas. *Space Science Reviews*, 42(1-2):153–167, 1985.
- [23] J. U. Brackbill and D. C. Barnes. The effect of nonzero Div B on the numerical solution of the magnetohydrodynamic equations. *Journal of Computational Physics*, 35(3):426–430, 1980.
- [24] S. C. Brenner and R. Scott. *The mathematical theory of finite element methods*, volume 15. Springer Science & Business Media, 2008.
- [25] S. C. Brenner and L.-Y. Sung. Virtual element methods on meshes with small edges or faces. *Mathematical Models & Methods in Applied Sciences*, 28(07):1291–1336, 2018.
- [26] F. Brezzi. On the existence, uniqueness and approximation of saddle-point problems arising from Lagrangian multipliers. *Rev. Française Automat. Informat. Recherche Opérationnelle Sér. Rouge*, 8(R-2):129–151, 1974.
- [27] F. Brezzi, A. Buffa, and K. Lipnikov. Mimetic finite differences for elliptic problems. *M2AN Math. Model. Numer. Anal.*, 43:277–295, 2009.
- [28] A. Cangiani, E. H. Georgoulis, T. Pryer, and O. J. Sutton. A posteriori error estimates for the virtual element method. *Numer. Math.*, 137:857–893, 2017.

- [29] A. Cangiani, V. Gyra, G. Manzini, and Sutton. O. Chapter 14: Virtual element methods for elliptic problems on polygonal meshes. In K. Hormann and N. Sukumar, editors, *Generalized Barycentric Coordinates in Computer Graphics and Computational Mechanics*, pages 1–20. CRC Press, Taylor & Francis Group, 2017.
- [30] A. Cangiani, G. Manzini, A. Russo, and N. Sukumar. Hourglass stabilization of the virtual element method. *Internat. J. Numer. Methods Engrg.*, 102(3-4):404–436, 2015.
- [31] O. Certik, F. Gardini, G. Manzini, L. Mascotto, and G. Vacca. The p- and hp-versions of the virtual element method for elliptic eigenvalue problems. *Comput. Math. Appl.*, 79(7):2035–2056, 2020.
- [32] O. Certik, F. Gardini, G. Manzini, and G. Vacca. The virtual element method for eigenvalue problems with potential terms on polytopic meshes. *Applications of Mathematics*, 63(3):333–365, 2018.
- [33] L. Chacón. An optimal, parallel, fully implicit Newton–Krylov solver for three-dimensional viscoresistive magnetohydrodynamics. *Physics of Plasmas*, 15(5):056103, 2008.
- [34] L. Beirão da Veiga, F. Brezzi, F. Dassi, LD Marini, and A. Russo. Lowest order virtual element approximation of magnetostatic problems. *Computer Methods in Applied Mechanics and Engineering*, 332:343–362, 2018.
- [35] L. Beirão Da Veiga, Franco Dassi, and Alessandro Russo. High-order virtual element method on polyhedral meshes. *Computers & Mathematics with Applications*, 74(5):1110–1122, 2017.
- [36] W. Dai and P. R. Woodward. On the divergence-free condition and conservation laws in numerical simulations for supersonic magnetohydrodynamical flows. *The Astrophysical Journal*, 494(1):317, 1998.
- [37] F. Dassi and L. Mascotto. Exploring high-order three dimensional virtual elements: bases and stabilizations. *Comput. Math. Appl.*, 75(9):3379–3401, 2018.
- [38] P. A. Davidson. An introduction to magnetohydrodynamics, 2002.
- [39] A. Dedner, F. Kemm, D. Kröner, C. D. Munz, T. Schnitzer, and M. Wesenberg. Hyperbolic divergence cleaning for the MHD equations. *Journal of Computational Physics*, 175(2):645–673, 2002.
- [40] D. A. Di Pietro, J. Droniou, and G. Manzini. Discontinuous skeletal gradient discretisation methods on polytopal meshes. *J. Comput. Phys.*, 355:397–425, 2018.
- [41] J. Ding and Y. Yang. Low-dispersive FDTD on hexagon revisited. *Electronics Letters*, 53(13):834–835, 2017.
- [42] S. C. Eisenstat and H. F. Walker. Choosing the forcing terms in an inexact Newton method. *SIAM Journal on Scientific Computing*, 17(1):16–32, 1996.
- [43] E. Emmrich. *Discrete versions of Gronwall’s lemma and their application to the numerical analysis of parabolic problems*. Techn. Univ., 1999.
- [44] E. G. Harris. On a plasma sheath separating regions of oppositely directed magnetic field. *Il Nuovo Cimento (1955-1965)*, 23(1):115–121, 1962.
- [45] K. Hu, Y. Ma, and J. Xu. Stable finite element methods preserving $\operatorname{div} B = 0$ exactly for MHD models. *Numerische Mathematik*, 135(2):371–396, 2017.
- [46] B. Jiang. *The least-squares finite element method: theory and applications in computational fluid dynamics and electromagnetics*. Springer Science & Business Media, 1998.
- [47] M. Joaquim and S. Scheer. Finite-difference time-domain method for three-dimensional grid of hexagonal prisms. *Wave Motion*, 63:32–54, 2016.
- [48] C. T. Kelley. *Iterative methods for linear and nonlinear equations*, volume 16. Siam, 1995.
- [49] M. G. Kivelson and C. T. Russell. *Introduction to space physics*. Cambridge university press, 1995.
- [50] D. Kuzmin and N. Klyushnev. Limiting and divergence cleaning for continuous finite element discretizations of the MHD equations. *Journal of Computational Physics*, 407:109230, 2020.
- [51] K. Lipnikov, G. Manzini, and M. Shashkov. Mimetic finite difference method. *J. Comput. Phys.*, 257 – Part B:1163–1227, 2014. Review paper.
- [52] J. G. Liu and W. C. Wang. An energy-preserving MAC–Yee scheme for the incompressible MHD equation. *Journal of Computational Physics*, 174(1):12–37, 2001.
- [53] J. G. Liu and W. C. Wang. Energy and helicity preserving schemes for hydro-and magnetohydro-dynamics flows with symmetry. *Journal of Computational Physics*, 200(1):8–33, 2004.
- [54] D. Loghin and A. J. Wathen. Analysis of preconditioners for saddle-point problems. *SIAM Journal on Scientific Computing*, 25(6):2029–2049, 2004.
- [55] G. Manzini, K. Lipnikov, J. D. Moulton, and M. Shashkov. Convergence analysis of the mimetic finite difference method for elliptic problems with staggered discretizations of diffusion coefficients. *SIAM J. Numer. Anal.*, 55(6):2956–2981, 2017.
- [56] G. Manzini, A. Russo, and N. Sukumar. New perspectives on polygonal and polyhedral finite element methods. *Math. Models Methods Appl. Sci.*, 24(8):1621–1663, 2014.
- [57] L. Mascotto. Ill-conditioning in the virtual element method: stabilizations and bases. *Numer. Methods Partial Differential Equations*, 34(4):1258–1281, 2018.
- [58] Peter Monk et al. *Finite element methods for Maxwell’s equations*. Oxford University Press, 2003.
- [59] D. Mora, G. Rivera, and R. Rodríguez. A virtual element method for the Steklov eigenvalue problem. *Math. Methods Appl. Sci.*, 25(08):1421–1445, 2015.
- [60] R. J. Moreau. *Magnetohydrodynamics*, volume 3. Springer Science & Business Media, 2013.
- [61] J. R. Munkres. *Analysis on manifolds*. CRC Press, 2018.
- [62] S. Naranjo-Alvarez, V. A. Bokil, V. Gyrya, and Manzini. G. A virtual element method for magnetohydrodynamics. *arXiv preprint arXiv:2004.11467*, 2020.

- [63] Sebastián Naranjo Álvarez. *Virtual Element Methods for Magnetohydrodynamics on General Polygonal and Polyhedral Meshes*. PhD thesis, Oregon State University, 2021.
- [64] G. H. Paulino and A. L. Gain. Bridging art and engineering using Escher-based virtual elements. *Struct. and Multidisciplinary Optim.*, 51(4):867–883, 2015.
- [65] I. Perugia, P. Pietra, and A. Russo. A plane wave virtual element method for the Helmholtz problem. *ESAIM Math. Model. Num.*, 50(3):783–808, 2016.
- [66] K. Schindler. *Physics of space plasma activity*. Cambridge University Press, 2006.
- [67] G. Tóth. The $\operatorname{div} B = 0$ constraint in shock-capturing magnetohydrodynamics codes. *Journal of Computational Physics*, 161(2):605–652, 2000.
- [68] G. Vacca. An H^1 -conforming virtual element for Darcy and Brinkman equations. *Mathematical Models & Methods in Applied Sciences*, 28(01):159–194, 2018.
- [69] P. Wriggers, W. T. Rust, and B. D. Reddy. A virtual element method for contact. *Comput. Mech.*, 58(6):1039–1050, 2016.

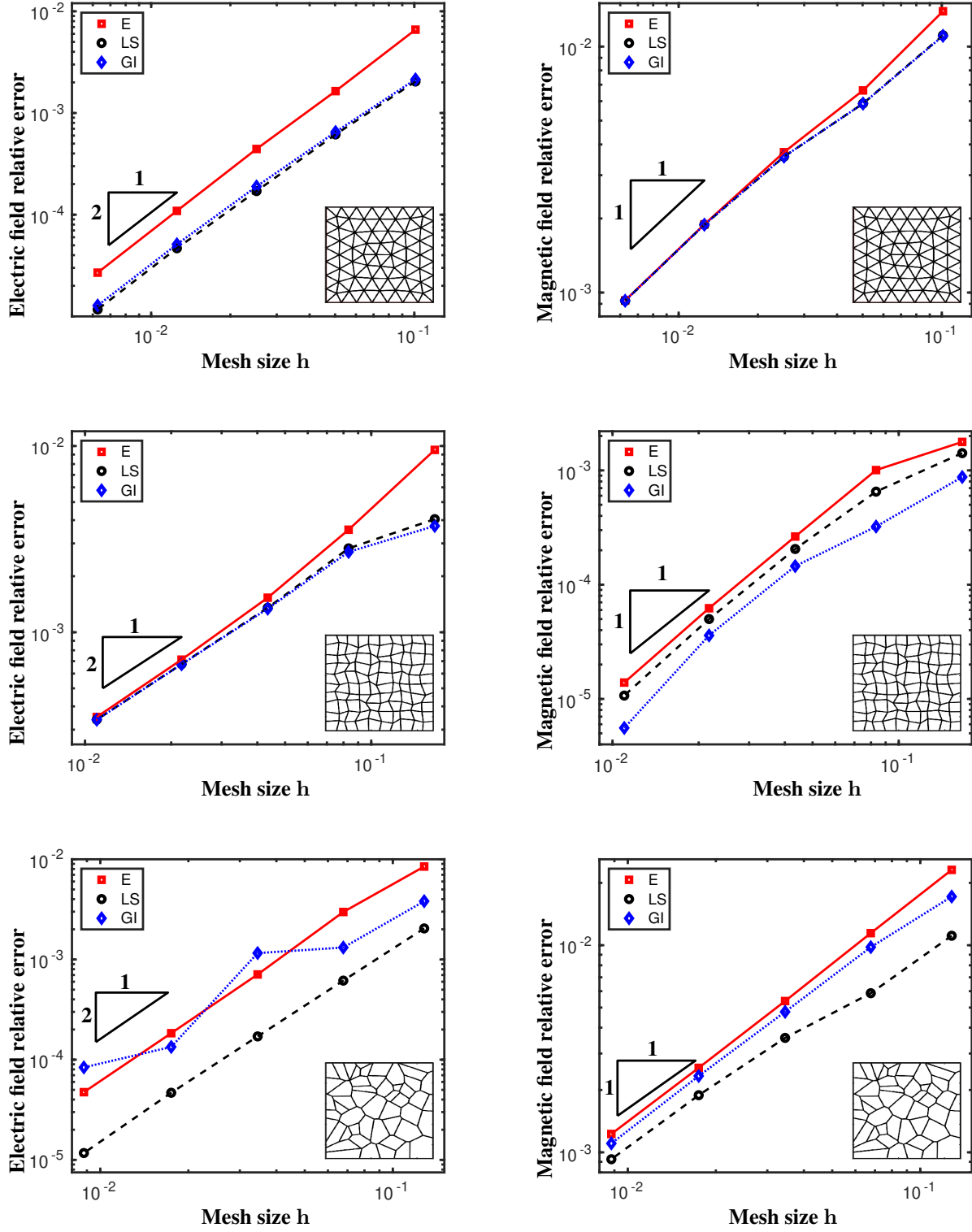


Fig. 5. Convergence plots of the VEM developed for the system (138). The type of mesh used in the simulation is portrayed in the lower right corner of each plot. The three convergence curves shown in each plot show the different performance between the three possibilities of the inner product in the space \mathcal{V}_h , see subsection 3.2.1. Each of these inner products is associated with a projector, they are the elliptic projector (E), the least squares projector (LS) and the Galerkin interpolator (GI).

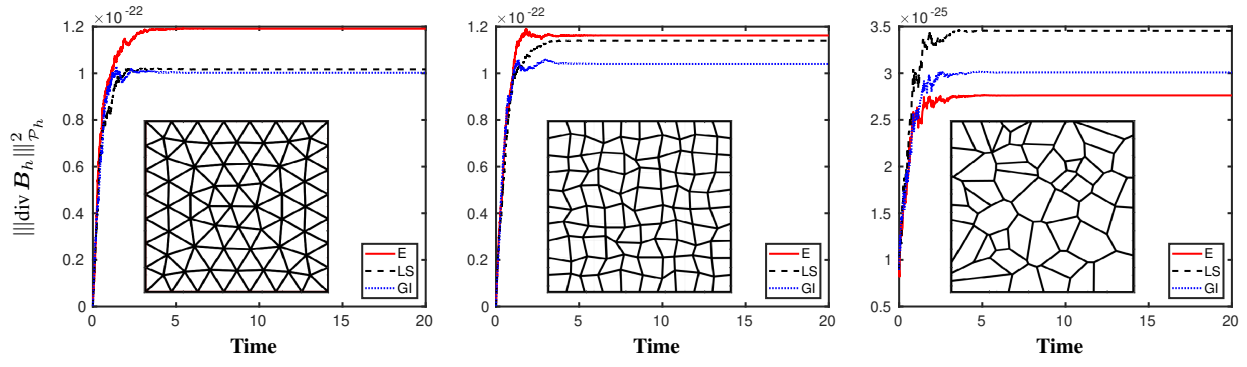


Fig. 6. Plots of the time evolution of the square of the L^2 norm of the divergence of the numerical magnetic field. We present three different types of meshes, these are displayed in the lower right hand corner of each plot.

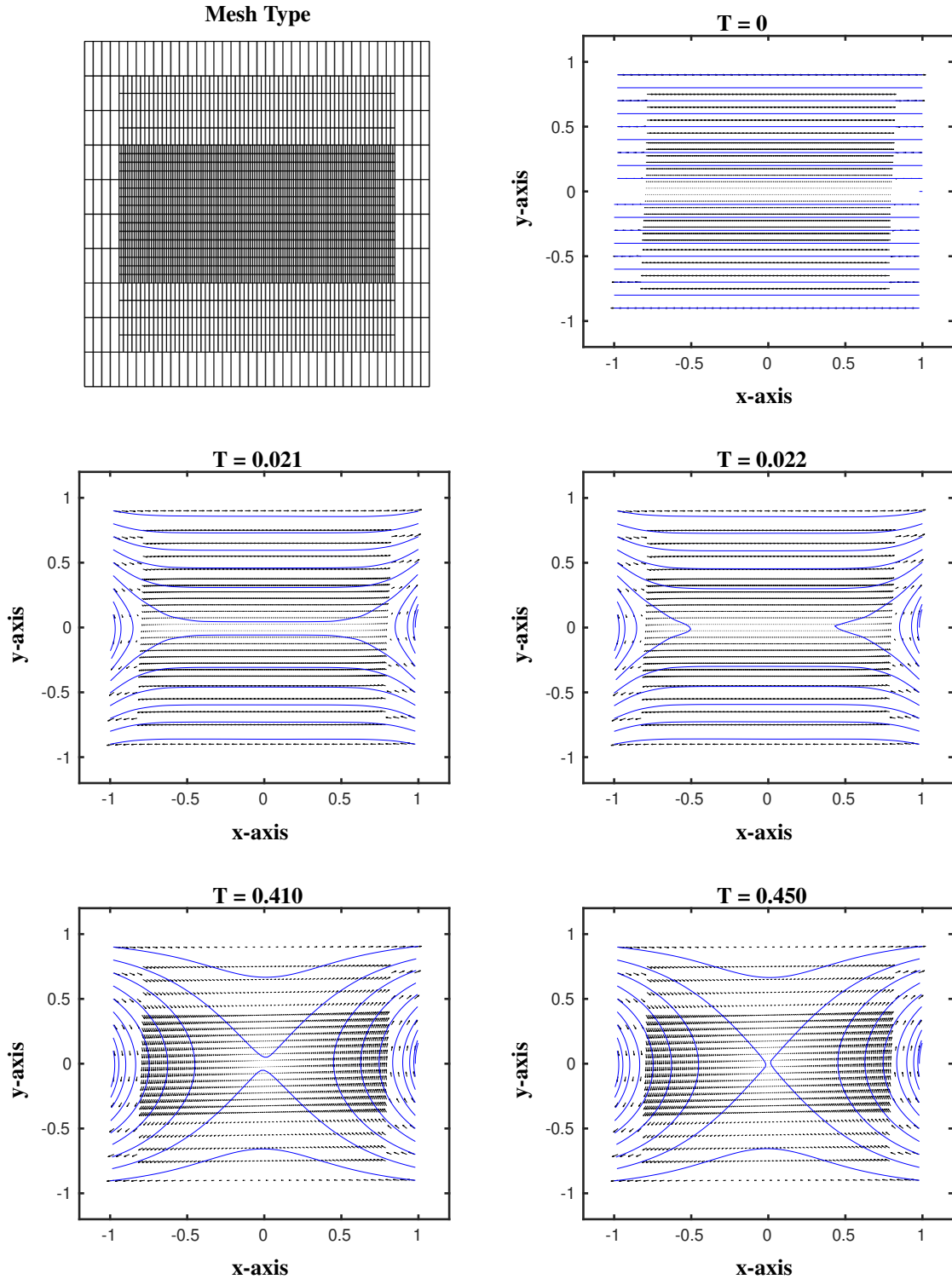


Fig. 7. Frames displaying the evolution, in time, of the magnetic field. The phenomenon of magnetic reconnection begins right away and by $T=0.450$ a steady state is achieved.